INTERNATIONAL JOURNAL FOR NUMERICAL AND ANALYTICAL METHODS IN GEOMECHANICS
Int. J. Numer. Anal. Meth. Geomech., 2005; **29**:751–787
Published online 26 April 2005 in Wiley InterScience (www.interscience.wiley.com). DOI: 10.1002/nag.434

A double structure generalized plasticity model for expansive materials

Marcelo Sánchez[1,‡], Antonio Gens[1,§], Leonardo do Nascimento Guimarães[2] and Sebastián Olivella[1,*,†]

[1] *Department of Geotechnical Engineering and Geosciences, Universitat Politécnica de Catalunya (UPC), Barcelona, Spain*
[2] *Universidade Federal de Pernambuco, Recife, Brazil*

SUMMARY

The constitutive model presented in this work is built on a conceptual approach for unsaturated expansive soils in which the fundamental characteristic is the explicit consideration of two pore levels. The distinction between the macro- and microstructure provides the opportunity to take into account the dominant phenomena that affect the behaviour of each structural level and the main interactions between them. The microstructure is associated with the active clay minerals, while the macrostructure accounts for the larger-scale structure of the material. The model has been formulated considering concepts of classical and generalized plasticity theories. The generalized stress–strain rate equations are derived within a framework of multidissipative materials, which provides a consistent and formal approach when there are several sources of energy dissipation. The model is formulated in the space of stresses, suction and temperature; and has been implemented in a finite element code. The approach has been applied to explaining and reproducing the behaviour of expansive soils in a variety of problems for which experimental data are available. Three application cases are presented in this paper. Of particular interest is the modelling of an accidental overheating, that took place in a large-scale heating test. This test allows the capabilities of the model to be checked when a complex thermo-hydro-mechanical (THM) path is followed.

KEY WORDS: constitutive modelling; expansive soils; unsaturated porous medium; fabric/structure of soils; suction

1. INTRODUCTION

The study of expansive soils has been a subject of increasing interest in recent research [1–6]. A major motivation is the possible use of those materials as engineered barriers and seals

*Correspondence to: Sebastián Olivella, Departamento de Ingeniería del Terreno, Universidad Politécnica de Catalunya, Jordi Girona 1-3, Edificio D-2, 08034 Barcelona, Spain.
† E-mail: sebastia.olivella@upc.es
‡ E-mail: marcelo.sanchez@upc.es
§ E-mail: antonio.gens@upc.es

Contract/grant sponsor: ENRESA
Contract/grant sponsor: European Commission
Contract/grant sponsor: CAPES
Contract/grant sponsor: Ministerio de Ciencia y Tecnología; contract/grant number: BTE 2001-2227

Received January 2004
Accepted December 2004

in radioactive waste repositories. Many disposal concepts consider the barrier made up from highly expansive compacted clay, in an initially unsaturated state. During its lifetime the barrier will undergo processes of heating, induced by the heat-emitting waste, and of hydration, coming from the host rock (which is generally in a saturated state). This scenario has led to increasing interest in the knowledge of the behaviour of unsaturated expansive soils under a wide range of testing conditions; in particular the thermo-hydro-mechanical (THM) behaviour has received special attention [7–12]. However, the interest on these materials is not limited to nuclear waste disposal applications, but they are present in other engineering problems such as shallow and deep foundations, slopes with stability problems, desiccation and formation of fissures in soils in arid regions, and clay based liners for waste isolation from the environment.

Comprehensive modelling of unsaturated expansive clays is a complex problem. The swelling behaviour of these clays has often been reproduced through relatively simple and empirical laws, which relate the material response to suction changes and applied stresses. There are relatively few formulations that integrate the main aspects of behaviour in a unified framework [13–15]. In that sense the approach proposed by Gens and Alonso [13] can be mentioned as a reference framework to analyse the behaviour of unsaturated expansive materials. In that work, particular attention is placed on the clay fabric and how it can be integrated in the constitutive modelling of the different structural levels present in an expansive soil.

The fabric of compacted expansive clay has been actively studied [6, 8, 16, 17], a marked double structure is generally observed. For instance, Figure 1 presents the results of mercury intrusion porosimeter tests of the FEBEX bentonite [6]. The two dominant pores size may be associated with two basic structural levels: (i) the macrostructure, composed by the global arrangements of clay aggregates, with macropores between them, and, (ii) the microstructure, which corresponds to the active clay minerals and their vicinity. Figure 2 shows a schematic representation of the conceptual model. Appendix A presents the phase diagram related to this conceptual model.

The model presented in this work is based on the general framework proposed by Gens and Alonso [13] and considers some of the improvements suggested in Reference [14]. A series of

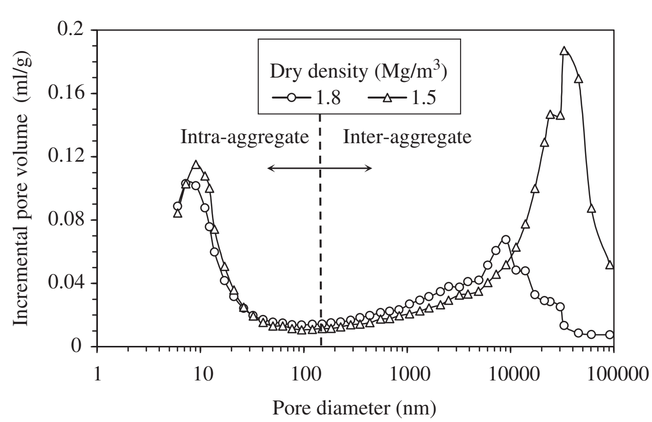

Figure 1. Distribution of incremental pore volume for two compacted bentonite samples at different dry densities. Mercury Intrusion Porosimeter test [6].

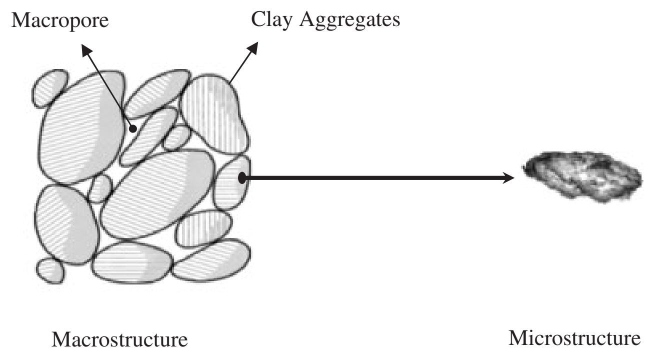

Figure 2. Schematic representation of the two structural levels considered.

modifications and developments have been performed in order to enhance the constitutive law and also to formulate the model in a form more suitable for its implementation in a finite element code. One of the aims is to provide a more general mathematical framework in order to achieve a more general interpretation of the phenomena that take place in expansive clays subjected to complex THM paths. To this end, concepts of generalized plasticity theory have been included in the formulation of the model. The governing small strain–stress equations have been derived considering concepts of multi-dissipative materials [18].

The mechanical law is the core of a double structure THM formulation specially developed to handle coupled THM problems in geological media. The double structure approach has been implemented in the finite element program CODE_BRIGHT [19] and has been applied to solve a number of boundary value problems [20]. This paper contains the description of the mechanical constitutive model, with the main aspects of the mathematical framework adopted, and includes three application cases. More details can be found in Reference [20].

In order not to clutter the main body of the paper, most mathematical derivations and detailed model expressions are collected in the appendices. In the following, bold faces indicate tensors; stresses ($\boldsymbol{\sigma}$) and strains ($\boldsymbol{\varepsilon}$) are considered as first-order tensors and stiffness and compliance matrices are second-order tensors.

2. MODEL FORMULATION

The microstructure is the seat of the basic physical–chemical phenomena occurring at clay particle level. These microstructural phenomena underlie many features of expansive soils behaviour [13]. In addition, deformations due to loading and collapse may have a major effect at macrostructural level. This macrostructural behaviour can be described by concepts and models of unsaturated non-expansive soils, such as the elasto-plastic Barcelona basic model (BBM) developed by Alonso *et al.* [21]. In expansive soils there are other mechanisms in addition to the ones included in the BBM which can induce plastic strains [13]. For example, Figure 3 shows the behaviour of compacted expansive clay subjected to a cyclic suction-controlled oedometer test with suctions varying between 0.2 and 1.7 MPa [22]. In this test the sample is subjected

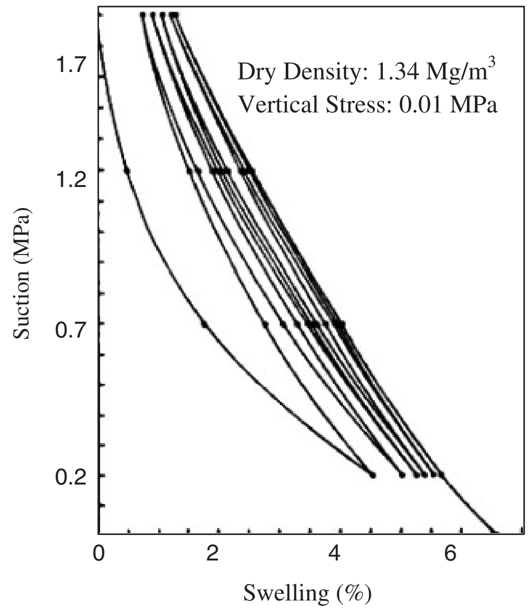

Figure 3. Accumulation of swelling strain in a cyclic suction test [22].

alternatively to wetting and drying paths under constant vertical stress. It can be observed that the material exhibits a clear non-linear behaviour, with irreversible accumulated deformations at the end of each cycle. The results obtained by Day [23] in a suction cyclic test (Figure 4) also show a marked inelastic behaviour. This is again a compacted clay, but here the amplitude of the suction cycles is wider, because the sample was dried under atmospheric conditions during the summer months in southern California. It is important to highlight that both samples were compacted under static conditions, and that the constant vertical stress applied during the test was relatively low. In this situation, it is expected that the observed plastic deformations were developed inside the macrostructural yield surface of the BBM. This inelastic behaviour can be associated with the interactions between the two structural levels. This plastic mechanism considers that microstructural changes can modify the global arrangement of aggregates in an irreversible way [13].

More experimental work related to the soil behaviour under suction cycles can be found in the literature (e.g. References [24–27]). Different techniques of suction control and different stress paths were applied by different authors. From those tests, two main aspects can be noted: irreversible behaviour appears independently of the suction level and, it is difficult to determine precisely the initiation of the yielding.

In this paper the elasto-plastic model related to the interaction mechanism between both structures is formulated in the framework of generalized plasticity theory. In this theory the yield function is not defined, at least in an explicit way. This theory is well suited if generalized stress reversals need to be modelled and also when there are several sources of energy dissipation [28–31]. A generalized plasticity model was applied to materials that show irrecoverable deformations upon reloading [32], and also to include the behaviour of soils under cyclic loading

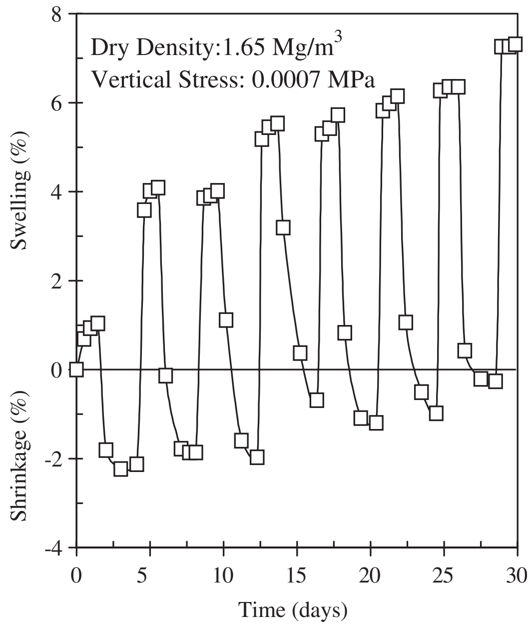

Figure 4. Evolution of shrinkage and swelling in a cyclic suction test [23].

when they exhibit irreversible deformation in loading, unloading and reloading [28, 29]. These are also typical aspects of behaviour observed in expansive soils under generalized stress paths including suction and stress changes.

There are significant advantages in using generalized plasticity theory to model the plastic mechanism related to the interaction between both pores structures. Some of them are:

- No clear evidence exists concerning the shapes of the internal yield surfaces corresponding to the interaction mechanisms between the two structural levels. Their experimental determination does not appear to be easy either.
- The effect of drying/wetting cycles on the behaviour of expansive soils is a matter of great practical importance. Generalized plasticity is especially well adapted to deal with this type of generalized cyclic loading.
- It is a formulation suitable to be implemented in numerical codes in a simple, robust and structured manner.
- It provides sufficient flexibility to incorporate additional microstructural phenomena such as non-equilibrium microstructural suction [20], or geochemical variables such as osmotic suction and cation exchange [33, 34].

Additionally, a generalized plasticity model is able to model a material behaviour characterized by the existence of an elastic domain (delimited by yield surfaces), since, the classical plasticity theory can be considered a particular case of the generalized plasticity theory [32, 35].

The model is formulated in terms of the three stress invariants (p, J, θ), suction (s) and temperature (T). The invariants are defined in Appendix B. The vector of generalized stresses, which includes temperature and suction, is identified with a hat, i.e.: $\hat{\boldsymbol{\sigma}} = \{T, s, p, J, \theta\}^{\mathrm{T}}$.

Finally, the complete model formulation requires the definition of laws for: (i) the macrostructural level, (ii) the microstructural level, and (iii) the interaction between the structural levels. In the following sections the main aspects of these three parts of the model are presented.

2.1. Macrostructural model

The BBM is able to reproduce many of the basic patterns of behaviour observed in non-expansive soils [21]. In that sense, it is an appropriate law to model the macrostructural behaviour. The BBM considers two independent stress variables to model the unsaturated behaviour, these are: the net stresses ($\boldsymbol{\sigma}$), computed as the excess of the total stresses over the gas pressure ($\boldsymbol{\sigma}_{\mathrm{t}} - \mathbf{I}p_{\mathrm{g}}$), and the matric suction (s), computed as the difference between gas pressure and liquid pressure ($p_{\mathrm{g}} - p_{\mathrm{l}}$). The BBM is an elasto-plastic strain-hardening model, which extends the concept of critical state for saturated soils to unsaturated conditions including a dependence of the yield surface on matric suction (Figure 5). The size of the yield surface increases with suction and the trace on the isotropic p–s plane is called the loading–collapse (LC) yield curve, because it represents the locus of activation of irreversible deformations due to loading increments or collapse (compression) due to wetting. The position of the LC curve is given by the value of the hardening variable p_0^*, which is the pre-consolidation yield stress of the saturated state.

Concerning the effects of temperature on clay behaviour, several constitutive laws have been developed to include the thermal effects under saturated conditions [36–40]. In this work, the effects of temperature have been integrated in the model in accordance with the thermo-mechanical law for non-saturated conditions proposed by Gens [41]. The thermal effect is included by considering that the elastic component of the strain induced by temperature changes is only volumetric and assuming a dependence of the pre-consolidation pressure on temperature. In this way, the fact that temperature increments reduce the size of the yield surface and the

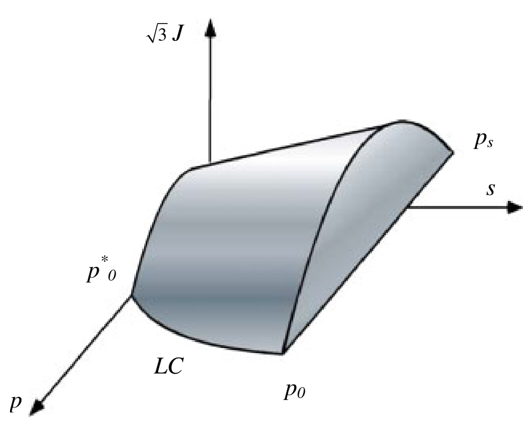

Figure 5. Three-dimensional representation of the BBM yield surface.

strength of the material is taken into account. This is a well-known behaviour for saturated conditions [36] that can also be extended to unsaturated conditions, as confirmed in recent experimental work [11, 12]. The global (macroscopic) thermal response of the material is considered at the macrostructural level.

A version of the modified Cam Clay model is the saturated law adopted as a limit condition of the unsaturated formulation [21]. The yield surface (F_{LC}) can be expressed as

$$F_{\mathrm{LC}} = 3J^2 - \left[\frac{g(\theta)}{g(-30^\circ)}\right]^2 M^2(p + p_{\mathrm{s}})(p_0 - p) = 0 \tag{1}$$

where M is the slope of the critical state, p_0 is the apparent unsaturated isotropic pre-consolidation pressure, g is a function of Lode's angle and p_{s} considers the dependence of shear strength on suction and temperature [41].

The hardening law is expressed as a rate relation between volumetric plastic strain and the saturated isotropic pre-consolidation stress, (p_0^*, Figure 5), according to

$$\frac{\dot{p}_0^*}{p_0^*} = \frac{(1+e)}{(\lambda_{(0)} - \kappa)}\dot{\boldsymbol{\varepsilon}}_v^{\mathrm{p}} \tag{2}$$

where e is void ratio, κ is the elastic compression index for changes in net mean stress and $\lambda_{(0)}$ is the compression index for changes in net mean stress for virgin states of the soil in saturated conditions.

Regarding the direction of the plastic strain increment, a non-associated flow rule in the plane $s = \text{constant}$ and $T = \text{constant}$ is suggested [21, 41]. The plastic potential (G) adopted is given by

$$G = \alpha 3J^2 - \left[\frac{g(\theta)}{g(-30^\circ)}\right]^2 M^2(p + p_{\mathrm{s}})(p_0 - p) = 0 \tag{3}$$

where α is determined from the condition that the flow rule predicts zero lateral strains in a K_0 stress path [21]. In Appendix B the main BBM equations are presented.

2.2. Microstructural model

It is assumed that physico-chemical phenomena occurring at this level are basically reversible and that the microstructural fabric does not have a preferential orientation [13]. So, the deformations arising from microstructural phenomena can be considered elastic and volumetric. The microstructural volumetric strain depends on a microstructural effective stress ($\hat{p}$) defined as [42]

$$\hat{p} = p + \chi s_{\mathrm{t}} \quad \text{where } s_{\mathrm{t}} = s + s_{\mathrm{o}} \tag{4}$$

where p is the net mean stress and s_{o} the osmotic suction. It is assumed that χ is a constant ($\chi > 0$). Here the total suction (s_{t}) is equal to the matric suction (s) because the effect of the osmotic suction is not considered. In References [33, 34] the formulation has been extended to include geochemical variables such as osmotic suction and cation exchange.

An additional assumption is made in the current formulation so that there is hydraulic equilibrium between the water potentials of the two structural levels (a similar hypothesis was made in (4)). This implies that the suctions associated to each of the water potentials are equal

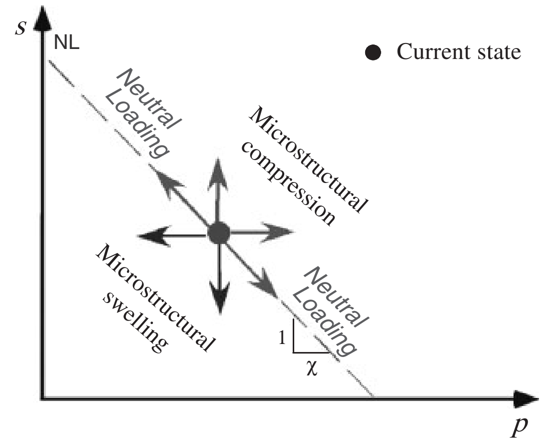

Figure 6. Definition of microstructural swelling and contraction directions.

and, therefore, only one suction variable should be considered. Therefore, in the model formulation, the generic name of suction (s) is used for both, but it has different physical meaning depending on the structural level considered. In Reference [20], an extension of the constitutive model to handle problems in which this hypothesis is relaxed is presented.

In the p–s plane, the line corresponding to constant microstructural effective stresses is referred to as the neutral line (F_{NL}) since no microstructural deformation occurs when the stress path moving on it, $\hat{p} = \text{constant}$ (Figure 6).

The neutral loading line (NL) divides the p–s plane into two parts, defining two main microstructural stress paths, which are identified as

$\dot{\hat{p}} > 0 \Rightarrow$ microstructural contraction (MC) path
$\dot{\hat{p}} < 0 \Rightarrow$ microstructural swelling (MS) path.

The increment of the microstructural elastic deformation is expressed as a function of the increment of the microstructural effective stress:

$$\dot{\boldsymbol{\varepsilon}}_{v\mathrm{m}} = \frac{\dot{\hat{p}}}{K_{\mathrm{m}}} = \frac{\dot{p}}{K_{\mathrm{m}}} + \chi \frac{\dot{s}}{K_{\mathrm{m}}} \tag{5}$$

where the subscript m refers to the microstructural level, the subscript v refers to the volumetric component and K_{m} is the microstructural bulk modulus (Appendix C).

2.3. Interaction between structural levels

Gens and Alonso [13] include the interaction between the two structural levels as a basic point of their approach, in order to achieve a more comprehensive description of expansive soil behaviour. The irreversible macrostructural deformations induced by microstructural effects are considered proportional to the microstructural strains according to interaction functions [13, 14]. In a general form it can be expressed as

$$\dot{\boldsymbol{\varepsilon}}^{\mathrm{p}}_{v\beta} = f\,\dot{\boldsymbol{\varepsilon}}_{v\mathrm{m}} \tag{6}$$

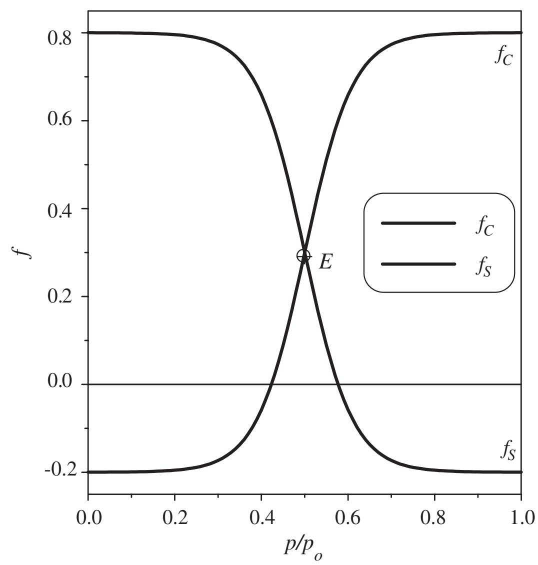

Figure 7. Interaction functions.

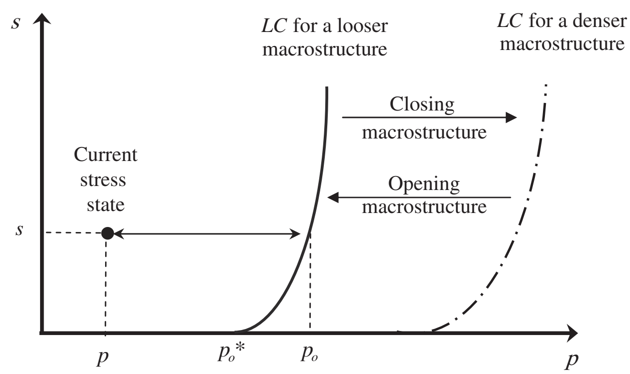

Figure 8. Movements of the LC yield curve due to microstructural effects.

where $\boldsymbol{\varepsilon}^{\mathrm{p}}_{v\beta}$ is the macrostructural plastic strain arising from the interaction mechanisms between both structures. Two interaction functions f are defined: f_{C} for MC paths and f_{S} for MS paths. In the case of isotropic loading, the interaction functions depend on the ratio p/p_0. Figure 7 shows a generic representation of the interaction functions.

The ratio p/p_0 is a measure of the degree of openness of the macrostructure relative to the applied stress state. When this ratio is low it implies a dense packing of the material (Figure 8). It is expected that under the latter condition (dense macrostructure) the microstructural swelling (MS path) affects strongly the global arrangements of clay aggregates, inducing large macrostructural plastic strains. So, the higher values of the f_{S} function correspond to low values of p/p_0. In this case the microstructure effects induce a more open macrostructure, which implies a macrostructural softening. On the other hand, when the microstructure contracts

(MC path) the larger (induced) macrostructural plastic strains occur with open macrostructures, that is, for values of p/p_0 close to 1. Under this path the clay tends to a more dense state, which implies a hardening of the macrostructure. This coupling between both plastic mechanisms is considered mathematically assuming that:

$$\dot{\boldsymbol{\varepsilon}}_v^{\mathrm{p}} = \dot{\boldsymbol{\varepsilon}}_{v\mathrm{LC}}^{\mathrm{p}} + \dot{\boldsymbol{\varepsilon}}_{v\beta}^{\mathrm{p}} \tag{7}$$

That is, the hardening variable of the macrostructure (p_0^*, Equation (2)) depends on the total plastic volumetric strains ($\boldsymbol{\varepsilon}_v^{\mathrm{p}}$), which is obtained from the sum of plastic volumetric strains induced by the BBM yielding ($\boldsymbol{\varepsilon}_{v\mathrm{LC}}^{\mathrm{p}}$), plus those arising from the interaction mechanisms between both structures ($\boldsymbol{\varepsilon}_{v\beta}^{\mathrm{p}}$).

This mechanical law is able to model the macropore invasion induced by microstructure expansion, when conditions of high confinement prevail (as reported by Komine and Ogata [4]), considering negative values of the function f_{S} for high values of p/p_0 [14]. In Figure 7 the point in which both interaction curves meet, indicated as E, is the equilibrium point. This point represents the state of the material for which no cumulative deformations are observed after cycles of suction changes [14].

It is noted that the material response will depend strongly on the direction of the microstructural stress path relative to the NL, which delimits two regions of different material behaviour. A proper modelling requires the definition of specific elasto-plastic laws for each domain in order to describe correctly the material behaviour according to the microstructural stress path followed (MC or MS). Generalized plasticity theory can deal with such conditions, allowing the consideration of two directions of different behaviour and the formulation of proper elasto-plastic laws for each region. According to that theory, for a complete model definition, it is necessary to provide: (i) a loading and unloading direction, (ii) a plastic flow direction, and (iii) a plastic modulus. These are described below.

2.3.1. Loading and unloading direction. At every point of the stress space two vectors may be defined, one indicates the microstructural compression direction and the other the microstructural swelling direction (equivalent to loading/unloading in conventional stress/strain formulations). The neutral line is considered as reference for the microstructural behaviour dividing the generalized stress space in two regions. From Equation (4), the neutral line is defined as (Figure 9):

$$F_{\mathrm{NL}} : p + \chi s - \hat{p}_{\mathrm{NL}} = 0 \tag{8}$$

Then, the microstructural compression direction can be obtained as

$$\hat{\mathbf{n}}_{\mathrm{C}} = \frac{\partial F_{\mathrm{NL}}}{\partial \hat{\boldsymbol{\sigma}}} = \{0, \chi, 1, 0, 0\}^{\mathrm{T}} \tag{9}$$

The opposite direction defines the microstructural swelling direction, which is expressed by

$$\hat{\mathbf{n}}_{\mathrm{S}} = \frac{\partial F_{\mathrm{NL}}}{\partial \hat{\boldsymbol{\sigma}}} = \{0, -\chi, -1, 0, 0\}^{\mathrm{T}} \tag{10}$$

In order to provide a generic expression for the plastic mechanisms induced in MC or MS paths, β will indicate the type of path followed. The following general expression is obtained:

$$\hat{\mathbf{n}}_{\beta} = \frac{\partial F_{\mathrm{NL}}}{\partial \hat{\boldsymbol{\sigma}}} = \omega_{\beta}\{0, \chi, 1, 0, 0\}^{\mathrm{T}} \tag{11}$$

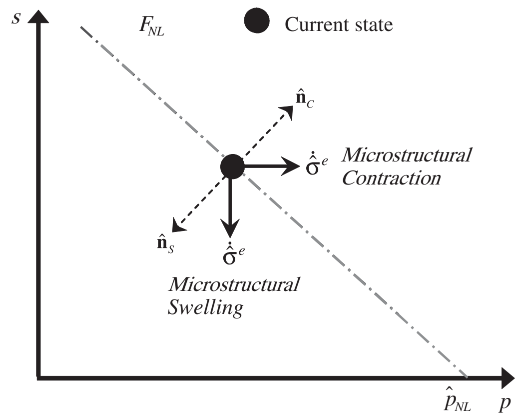

Figure 9. Definition of microstructural swelling and contraction directions.

where

$$\omega_\beta = 1 \quad \text{if } \beta = \mathrm{C} \quad \text{(MC path)} \tag{12}$$

$$\omega_\beta = -1 \quad \text{if } \beta = \mathrm{S} \quad \text{(MS path)} \tag{13}$$

Given a generalized stress state and a generalized stress increment, the criterion to identify the microstructural stress path can be specified as (Figure 9)

Microstructural compression criterion:

$$\hat{\mathbf{n}}_{\mathrm{C}}^{\mathrm{T}} \cdot \dot{\hat{\boldsymbol{\sigma}}}^{\mathrm{e}} > 0 \quad \text{(MC path)} \tag{14}$$

Microstructural swelling criterion:

$$\hat{\mathbf{n}}_{\mathrm{S}}^{\mathrm{T}} \cdot \dot{\hat{\boldsymbol{\sigma}}}^{\mathrm{e}} > 0 \quad \text{(MS path)} \tag{15}$$

Neutral loading:

$$\hat{\mathbf{n}}_{\beta}^{\mathrm{T}} \cdot \dot{\hat{\boldsymbol{\sigma}}}^{\mathrm{e}} = 0 \quad \text{(NL path)} \tag{16}$$

where $\dot{\hat{\boldsymbol{\sigma}}}^{\mathrm{e}}$ is the elastic generalized stress increment. The dot in Equations (14)–(16) means matrix product (single contraction in index notation).

2.3.2. Plastic flow direction. The concept of image point is applied to define the flow rule for a generic state. The image point is obtained as a projection of the current stress state on the BBM yield surface (Figure 10). It is assumed that the current stress ratio (η), θ, s and T are maintained constant during projection. The normal to the plastic potential at the image point ($\mathbf{n}_{G\otimes}$) is defined as

$$\mathbf{n}_{G\otimes} = \left(\frac{\partial G}{\partial p^{\otimes}}, \frac{\partial G}{\partial J^{\otimes}}, \frac{\partial G}{\partial \theta^{\otimes}}\right)^{\mathrm{T}} \tag{17}$$

The equations used to evaluate this vector and the projections are included in Appendix D. In order to define the flow rule it is necessary to take into account the component of

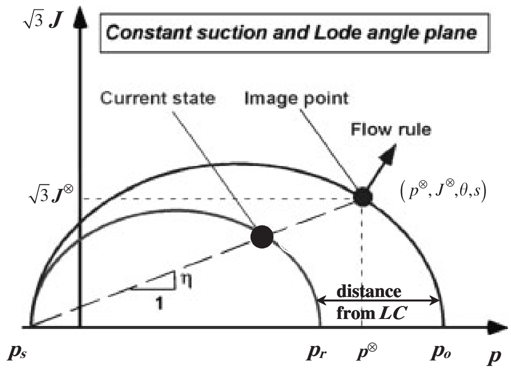

Figure 10. Reference pressure and plastic flow direction.

macrostructural behaviour induced by microstructural strains due to the coupling mechanism. For a given microstructural path (MC or MS), the macrostructural response (expansion or compression) depends on the sign of the interaction function f_β. If f_β is positive the effect on the macrostructure goes in the same direction as the microstructural deformation. When f_β is negative, the opposite occurs. As an example, a microstructural compression path is examined. This path leads to a contracting behaviour of the microstructure. Therefore if f_C is positive, the macrostructure will also contract and macrostructural hardening will take place. In contrast, if f_C is negative, there will be expansive macrostructural strains and macrostructural softening will occur. To take into account these two possibilities, the flow rule for microstructure compression paths is finally given as

$$\mathbf{m}_\mathrm{C} = \frac{f_\mathrm{C}}{|f_\mathrm{C}|}\mathbf{n}_{G*} \tag{18}$$

where $\mathbf{m}_\mathrm{C}$ is the plastic flow direction. Similar considerations for microstructure swelling paths lead to:

$$\mathbf{m}_\mathrm{S} = \frac{f_\mathrm{S}}{|f_\mathrm{S}|}\mathbf{n}_{G*} \tag{19}$$

A general form of the plastic flow direction can be written as

$$\mathbf{m}_\beta = \omega_\beta \frac{f_\beta}{|f_\beta|}\mathbf{n}_{G*} \tag{20}$$

2.3.3. Plastic modulus. The plastic modulus (H_β) is defined adopting a similar structure as the one proposed by Pastor *et al.* [29]:

$$H_\beta = H_\beta^1 H_\beta^2 H_\beta^3 \tag{21}$$

where

(a) H_β^1 is the term that contains the main variables that control the coupling between both structures. It can be defined as

$$H_\beta^1 = \frac{K_\mathrm{m}}{f_\beta} \tag{22}$$

When the stress path is isotropic f_β depends on p/p_0. However, if a deviatoric stress component is applied f_β depends on the p_r/p_0 ratio (see Figure 10) and the following equation should be used to determine the distance to the LC surface:

$$p_r = p + \left[\frac{g(-30°)}{g(\theta)}\right]^2 \frac{3J^2}{M^2(p+p_s)} \tag{23}$$

where p_r is a reference mean net stress for a non-isotropic stress state. Figure 10 shows a schematic representation for this case.

(b) H_β^2 is the term that considers the history of the material associated to this mechanism. When it is assumed that irreversible macrostructural plastic strains are always induced by the microstructural effective stresses change, this factor is given by

$$H_\beta^2 = 1 \tag{24}$$

This implies that there is no elastic domain associated with the interaction mechanism. In this case a history variable ($\hat{p}_{NL}$), related to the last generalized microstructural stress reached by the material is considered (Figure 9).

At this point it is possible to introduce different evolution laws that take into account the history of the material. For example, a hypothetical case with an elastic domain has been modelled in Reference [20] following a similar approach to the one introduced in Reference [35]. In that case there were two yield surfaces, one for each microstructural stress path (MC or MS), delimiting the elastic behaviour. That is, a conceptual model similar to the one adopted in the Barcelona Expansive Model (BExM) [14].

(c) H_β^3 is a factor that ensures the correct scaling of the plastic deformations, and it is defined as

$$H_\beta^3 = \|\mathbf{m}_\beta\| \tag{25}$$

where $\|\mathbf{m}_\beta\|$ is the Euclidean norm of the vector.

Finally, the plastic strain increment induced by the β mechanism is integrated in the model considering these three basic elements of the generalized plasticity theory (Appendix E). The equation for the plastic strain increment caused by a stress increment is expressed as

$$\dot{\boldsymbol{\varepsilon}}_\beta^{\mathrm{p}} = \dot{\lambda}_\beta\, \mathbf{m}_\beta \tag{26}$$

where $\dot{\lambda}_\beta$ is defined in a similar way as in Reference [29], i.e.:

$$\dot{\lambda}_\beta = \frac{\mathbf{n}_\beta^{\mathrm{T}} \cdot \dot{\boldsymbol{\sigma}}}{H_\beta} \tag{27}$$

where $\mathbf{n}_\beta = \partial F_{NL}/\partial \boldsymbol{\sigma}$. Finally, after some algebraic combination of the equations above (Equation (6) for plastic strain, Equation (20) for flow rule, and, Equation (21) for plastic modulus), it is possible to obtain the volumetric strain increment due to a p increment for the component of plastic strain arising from the interactions mechanism:

$$\dot{\varepsilon}_{v\beta}^{\mathrm{p}} = f_\beta \frac{\dot{p}}{K_m} m_{v\beta} \tag{28a}$$

where

$$m_{v\beta} = \frac{\omega_\beta}{\|\mathbf{m}_\beta\|} \frac{f_\beta}{|f_\beta|} \frac{\partial G}{\partial p^\otimes} \tag{28b}$$

Equation (28a) expresses the coupling between structural levels as defined by Equations (5) and (6). The active mechanism (β) is identified according with the criterion of microstructural contraction/swelling established in Section 2.3.1 (Equations (14)–(16)).

In summary, the mechanical law has been formulated considering an elasto-plastic model (formulated in the context of classical plasticity) for the description of the macrostructural behaviour, a non-linear elastic model to describe the microstructural behaviour and a generalized plasticity model to include the irreversible effects induced by the coupling between both structural levels. The aim of the following section is to obtain the elasto-plastic tensors related to the increment of strains, suction and temperature, that define the stress–strain relations.

3. ELASTO-PLASTIC STRESS–STRAIN RELATIONS

The behaviour of the soil described by the double structure model can be regarded as the consequence of the joint action of several mechanisms that can act simultaneously. In this work, some concepts of multi-dissipative materials introduced by Rizzi *et al.* [18] have been considered to take into account that different mechanisms can induce plastic deformations. A first step is the assumption of an additive decomposition of the strains into elastic and plastic components; so, the increment of total strains can be expressed as

$$\dot{\boldsymbol{\varepsilon}} = \dot{\boldsymbol{\varepsilon}}^{\mathrm{e}} + \sum_{n=1}^{n=n_{\mathrm{a}}} \dot{\boldsymbol{\varepsilon}}_n^{\mathrm{p}} \tag{29}$$

where n_{a} is the number of active plastic mechanisms that correspond to one subset of the total plastic possible mechanisms. The model has three inelastic mechanisms: lc, due to yield of the BBM, and mc or ms when one of the two interaction mechanisms is active. Two is the maximum number of simultaneous active plastic mechanisms i.e. lc plus mc or ms.

In classical plasticity theory, it is assumed that the material behaves either as an elastic or a plastic solid. The yield surface defines the transition from elasticity to plasticity, stress states inside the yield surface are considered as elastic ($F<0$). In generalized plasticity theory the state of the material is determined from the control variables: generalized stresses, strains and a finite number of internal variables. A process of loading is defined as elastic if the set of internal variables remains unchanged [32].

In the case of elastic loading, the stress increment is related to the increment of strains, suction and temperature by the following relation:

$$\dot{\boldsymbol{\sigma}} = \mathbf{D}_{\mathrm{e}} \cdot \dot{\boldsymbol{\varepsilon}}^{\mathrm{e}} + \boldsymbol{\alpha}_{\mathrm{s}} \dot{s} + \boldsymbol{\alpha}_T \dot{T} \tag{30}$$

where $\mathbf{D}_{\mathrm{e}}$ is the global elastic matrix which considers the elastic component of the two structural levels. $\boldsymbol{\alpha}_{\mathrm{s}}$ and $\boldsymbol{\alpha}_{\mathrm{T}}$ are the elastic vectors associated with suction and temperature, respectively. The expressions for the elastic tensors are introduced in Appendices C and E. When a loading process is inelastic, plastic strain rates are assumed to be governed by a flow rule. For the macrostructural model, the strain increment can be expressed as

$$\dot{\boldsymbol{\varepsilon}}^{\mathrm{p}}_{\mathrm{LC}} = \dot{\lambda}_{\mathrm{LC}} \frac{\partial G}{\partial \boldsymbol{\sigma}} = \dot{\lambda}_{\mathrm{LC}} \mathbf{m}_{\mathrm{LC}} \tag{31}$$

where $\dot{\lambda}_{\mathrm{LC}}$ is the plastic multiplier associated to the lc plastic mechanism, and $\mathbf{m}_{\mathrm{LC}}$ is the flow rule direction (normal to the plastic potential, Equation (3)).

In this model the material behaviour is described by elasto-plastic mechanisms that can be activated during the loading process. The set of active plastic mechanisms is not known in advance. Therefore it is necessary to use an iterative procedure to find them [43, 44]. A possibility is to assume that all the plastic mechanisms are initially active [43]. Here it is assumed that both plastic mechanisms are initially active: lc and β (that is mc or ms).

Regarding the lc plastic mechanism it is assumed that once yield occurs (that is $F_{\mathrm{LC}} = 0$), the stresses must remain on the yield surface during plastic deformation. This constraint is enforced by the consistency condition, which implies that: $\dot{F}_{\mathrm{LC}} = 0$. After some algebra on the consistency condition (Appendix E), the following equation is obtained:

$$\dot{\lambda}_{\mathrm{LC}}(H_{\mathrm{LC}} + H^{\mathrm{c}}_{\mathrm{LC}}) + \dot{\lambda}_{\beta}(h_{\beta} + h^{\mathrm{c}}_{\beta}) = \dot{e}_{\mathrm{LC}} + \dot{s}_{\mathrm{LC}} + \dot{t}_{\mathrm{LC}} \tag{32}$$

where $\dot{\lambda}_{\mathrm{LC}}$ and $\dot{\lambda}_{\beta}$ are the unknowns. H_{LC}, $H^{\mathrm{c}}_{\mathrm{LC}}$, h_{β} and h^{c}_{β} are moduli related to the lc and β mechanisms, whereas, $\dot{e}_{\mathrm{LC}}$, $\dot{s}_{\mathrm{LC}}$ and $\dot{t}_{\mathrm{LC}}$ are variables linked to the increment of strains, suction and temperature. In Appendix E all the details of Equation (32) are presented.

For the β plastic mechanism, a procedure similar to that suggested by Pastor *et al.* [29] has been followed to obtain the equation with the unknowns $\dot{\lambda}_{\mathrm{LC}}$ and $\dot{\lambda}_{\beta}$. It can be written as

$$\dot{\lambda}_{\mathrm{LC}} h^{\mathrm{c}}_{\mathrm{LC}} + \dot{\lambda}_{\beta}(H_{\beta} + H^{\mathrm{c}}_{\beta}) = \dot{e}_{\beta} + \dot{s}_{\beta} + \dot{t}_{\beta} \tag{33}$$

where $h^{\mathrm{c}}_{\mathrm{LC}}$, H_{β} and H^{c}_{β} are moduli related to the plastic mechanisms (lc and β), and $\dot{e}_{\beta}$, $\dot{s}_{\beta}$ and $\dot{t}_{\beta}$ are variables linked to the increment of strains, suction and temperature. Appendix E contains additional details for the calculation of Equation (33).

The system formed by Equations (32) and (33) can be written as

$$\begin{aligned} \dot{\lambda}_{\mathrm{LC}} \bar{H}_{\mathrm{LC}} + \dot{\lambda}_{\beta} \bar{h}_{\beta} &= \dot{e}_{\mathrm{LC}} + \dot{s}_{\mathrm{LC}} + \dot{t}_{\mathrm{LC}} \\ \dot{\lambda}_{\mathrm{LC}} \bar{h}_{\mathrm{LC}} + \dot{\lambda}_{\beta} \bar{H}_{\beta} &= \dot{e}_{\beta} + \dot{s}_{\beta} + \dot{t}_{\beta} \end{aligned} \tag{34}$$

which can be expressed in a compact form as

$$\bar{\mathbf{H}} \cdot \dot{\boldsymbol{\lambda}} = \dot{\mathbf{e}} + \dot{\mathbf{s}} + \dot{\mathbf{t}}, \quad \bar{\mathbf{H}} = \mathbf{H} + \mathbf{H}^{\mathrm{c}} \tag{35}$$

The hardening modulus matrix ($\mathbf{H}$) is symmetric when there is reciprocity in the hardening rules of both mechanisms (reciprocal hardening implies that $H_{ij} = H_{ji}$ for $i \neq j$) [18]. So, this model has non-reciprocal hardening (h_{β} can be non-zero), because the only coupling between both plastic mechanisms is given by the hardening law of the BBM (Equations (5) and (6)).

According to Rizzi *et al.* [18], there is a unique increment of $\boldsymbol{\varepsilon}$ for any increment of $\boldsymbol{\sigma}$ if, and only if, $\mathbf{H}$ is a *P-matrix* (Appendix F). When this condition is satisfied, the flow rule of the multidissipative materials exhibits hardening, otherwise it exhibits softening. Finally, for $\mathbf{H} = 0$ the behaviour is perfectly plastic. For the general case of non-associative plasticity, there is a unique increment of $\boldsymbol{\sigma}$ for any increment of $\boldsymbol{\varepsilon}$, if, and only if, the effective hardening matrix $\bar{\mathbf{H}}$ is a *P-matrix*. $\mathbf{H}^{\mathrm{c}}$ is the critical softening matrix.

The assumption that $\bar{\mathbf{H}}$ is a *P-matrix* implies that each diagonal element of the $\mathbf{H}$ matrix plus the corresponding diagonal element of the $\mathbf{H}^{\mathrm{c}}$ matrix is greater than zero (i.e. $(H_{\mathrm{LC}} + H^{\mathrm{c}}_{\mathrm{LC}}) > 0$ and $(H_{\beta} + H^{\mathrm{c}}_{\beta}) > 0$). Therefore, the condition of $\bar{H} > 0$ is satisfied for each plastic mechanism. The solution of system (34) requires the inversion of the $\bar{\mathbf{H}}$ matrix which is assumed to be a *P-matrix*, obtaining:

$$\dot{\boldsymbol{\lambda}} = \bar{\mathbf{H}}^{-1} \cdot (\dot{\mathbf{e}} + \dot{\mathbf{s}} + \dot{\mathbf{t}}) \tag{36}$$

The choice of the plastic mechanisms initially assumed active should be verified by checking that they are actually active [43, 44]. If one of them is not active, the case becomes a single dissipative model.

The net stress increment can be expressed as

$$\dot{\boldsymbol{\sigma}} = \mathbf{D}_{\mathrm{e}} \cdot \left(\dot{\boldsymbol{\varepsilon}} - \dot{\boldsymbol{\varepsilon}}^{\mathrm{e}}_{\mathrm{s}} - \dot{\boldsymbol{\varepsilon}}^{\mathrm{e}}_{T} - \sum_{n=1}^{n=n_{\mathrm{a}}} \boldsymbol{\varepsilon}^{\mathrm{p}}_{n} \right) \tag{37}$$

After some algebra (Appendix E) the following general form is obtained:

$$\dot{\boldsymbol{\sigma}} = \mathbf{D}_{\mathrm{ep}} \cdot \dot{\boldsymbol{\varepsilon}} + \boldsymbol{\gamma}_{\mathrm{s}} \dot{s} + \boldsymbol{\gamma}_{T} \dot{T} \tag{38}$$

In the case of two active plastic mechanisms these tensors may be evaluated by

$$\mathbf{D}_{\mathrm{ep}} = \mathbf{D}_{\mathrm{e}} \cdot \left[\mathbf{I} - \frac{1}{|\bar{\mathbf{H}}|} (\bar{H}_{\beta} \mathbf{m}_{\mathrm{LC}} \cdot \mathbf{n}^{\mathrm{T}}_{\mathrm{LC}} - \bar{h}_{\beta} \mathbf{m}_{\mathrm{LC}} \cdot \mathbf{n}^{\mathrm{T}}_{\beta} + \bar{H}_{\mathrm{LC}} \mathbf{m}_{\beta} \cdot \mathbf{n}^{\mathrm{T}}_{\beta} - \bar{h}_{\mathrm{LC}} \mathbf{m}_{\beta} \cdot \mathbf{n}^{\mathrm{T}}_{\mathrm{LC}}) \cdot \mathbf{D}_{\mathrm{e}} \right] \tag{39}$$

$$\begin{aligned} \boldsymbol{\gamma}_{\mathrm{s}} = {} & \boldsymbol{\alpha}_{\mathrm{s}} + \boldsymbol{\beta}_{\mathrm{s}} - \frac{1}{|\bar{\mathbf{H}}|} \mathbf{D}_{\mathrm{e}} \cdot \{ \bar{H}_{\beta} \mathbf{m}_{\mathrm{LC}} [l + l_{\beta} + \mathbf{n}^{\mathrm{T}}_{\mathrm{LC}} \cdot (\boldsymbol{\alpha}_{\mathrm{s}} + \boldsymbol{\beta}_{\mathrm{s}})] - \bar{h}_{\beta} \mathbf{m}_{\mathrm{LC}} \mathbf{n}^{\mathrm{T}}_{\beta} \cdot (\boldsymbol{\alpha}_{\mathrm{s}} + \boldsymbol{\beta}_{\mathrm{s}}) \\ & + \bar{H}_{\mathrm{LC}}\, \mathbf{m}_{\beta} \mathbf{n}^{\mathrm{T}}_{\beta} \cdot (\boldsymbol{\alpha}_{\mathrm{s}} + \boldsymbol{\beta}_{\mathrm{s}}) - \bar{h}_{\mathrm{LC}} \mathbf{m}_{\beta} [l + l_{\beta} + \mathbf{n}^{\mathrm{T}}_{\mathrm{LC}} \cdot (\boldsymbol{\alpha}_{\mathrm{s}} + \boldsymbol{\beta}_{\mathrm{s}})] \} \end{aligned} \tag{40}$$

$$\begin{aligned} \boldsymbol{\gamma}_{T} = {} & \boldsymbol{\alpha}_{T} - \frac{1}{|\bar{\mathbf{H}}|} \mathbf{D}_{\mathrm{e}} \cdot [\bar{H}_{\beta} \mathbf{m}_{\mathrm{LC}} (d + \mathbf{n}^{\mathrm{T}}_{\mathrm{LC}} \cdot \boldsymbol{\alpha}_{T}) - \bar{h}_{\beta} \mathbf{m}_{\mathrm{LC}} \mathbf{n}^{\mathrm{T}}_{\beta} \cdot \boldsymbol{\alpha}_{T} + \bar{H}_{\mathrm{LC}} \mathbf{m}_{\beta} \mathbf{n}^{\mathrm{T}}_{\beta} \cdot \boldsymbol{\alpha}_{T} \\ & - \bar{h}_{\mathrm{LC}} \mathbf{m}_{\beta} (d + \mathbf{n}^{\mathrm{T}}_{\mathrm{LC}} \cdot \boldsymbol{\alpha}_{T})] \end{aligned} \tag{41}$$

Appendix E contains details to compute the elastic and elasto-plastic tensors. For simpler cases, for example when only the lc plastic mechanism is active a procedure similar to the one presented in Reference [41] has been followed. Conversely, when only the plastic mechanism β is active, the stress–strain rate equations have been obtained in accordance with the concepts of generalized plasticity presented in Reference [29]. More details can be found in Reference [20].

The mechanical model has been implemented in the finite element program CODE_BRIGHT, a numerical tool designed to handle coupled THM problems in geological media [19, 45]. A detailed description of the integration algorithm can be found in Reference [20].

4. APPLICATION CASES

The constitutive model has been applied to solve a variety of problems in which expansive soils are involved [20]. In this section, three cases are presented. The first case corresponds to the simulation of a swelling pressure test. The second example refers to a test involving wetting/drying cycles. The third one is related to the modelling of compacted bentonite behaviour under a complex THM path.

4.1. Swelling pressure test

The swelling pressure test offers valuable information related to the behaviour of expansive soils. In this section the simulation of a test carried out by Romero [8] on a sample of Boom clay pellets is presented. In these materials two structural levels can be clearly distinguished: the microstructure associated to the high density pellets (dry density $1.96\ \mathrm{mg/m^3}$); and the macrostructure that corresponds to the granular-like arrangement of these pellets (dry density $1.37\ \mathrm{mg/m^3}$) with macropores between the pellets. Table I presents the values of soil parameters and initial values of state variables used in the modelling.

The main objective of this simulation is to explain and reproduce the observed behaviour during the test (Figure 11). Therefore, a numerical analysis has been carried out prescribing the same suction changes as in the test under constant volume conditions. Figure 12 shows the computed vertical net stress–suction path. The initial condition (I) corresponds to an initial suction of 80 MPa and a low vertical stress and it is located inside the elastic domain. A wetting path is then followed up to a value of suction close to 0.01 MPa (point W). Finally the sample is subjected to drying, up to a maximum suction of 0.4 MPa. It can be observed that the model can reproduce satisfactorily the main trends observed during the test. Figure 13 shows the evolution of the BBM hardening parameter during the test and Figure 14 displays the evolution of the interaction functions f_C and f_S.

In the first stage (I–C) the stresses remains inside the LC yield surface and the stress path is determined by the increase of load required to compensate the swelling strains due to suction reduction. The ms mechanism is active with positive values of the f_S function during most of this stage. This implies that the induced macrostructural plastic strains (due to ms mechanism) are of expansion, with a tendency to a more open macrostructure and, consequently, a reduction of p_0^*. The LC yield curve moves to the left, from the initial position LC_I to the contact condition LC_C (i.e. a macrostructural softening). Negative values of f_S are in fact computed at the end of the I–C path (i.e. at high pressure, close to collapse) that result in the very slight change of tendency of p_0^* just before reaching point C. Point C corresponds to the contact point between

Table I. Parameters used to define the elasto-plastic constitutive law (Section 4.1).

Parameters defining the Barcelona basic model for macrostructural behaviour						
$\kappa = 0.020$	$\kappa_s = 0.010$	$\lambda_{(0)} = 0.650$	p_c (MPa) $= 0.01$	$r = 0.780$	ζ (MPa^{-1}) $= 5.00$	p_0^* (MPa) $= 0.11$
Parameters defining the law for microstructural behaviour						
$\kappa_m = 0.10$	$\chi = 1$					
Interaction functions						
$f_C = -0.10 + 1.10(p_r/p_0)^{0.5}$;	$f_S = -0.10 + 1.1(1 - p_r/p_0)^2$					
$e_{macro} = 0.60$	$e_{micro} = 0.35$					

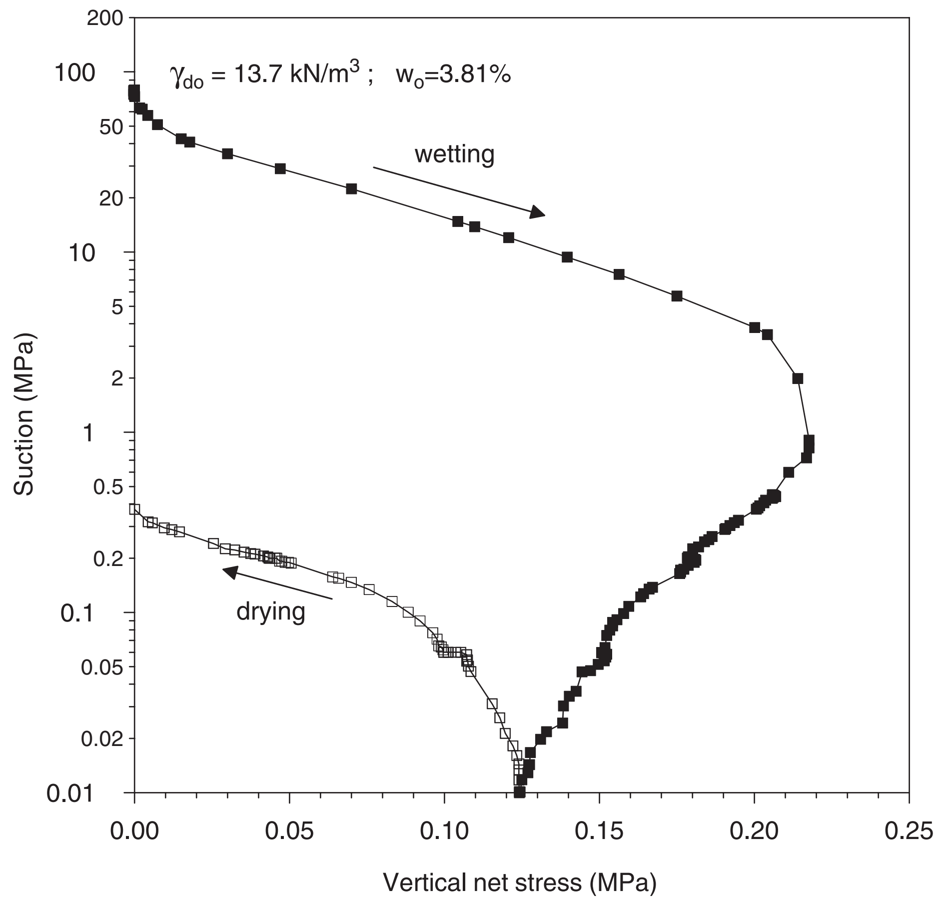

Figure 11. Reported stress path in the σ_v–s plane [8].

the stress path and the LC curve. Under this condition a collapse of the macrostructure occurs and the stresses tend to reduce to compensate the compression strains. This implies a hardening of the material with a significant increase of p_0^* (Figure 13). Now the stress path, on the p–s plane, is controlled by the shape of the LC curve, with both plastic mechanisms active (lc and β). Finally, during the drying path W–D the mc mechanism is active with positive values of f_C during a major part of this stage, inducing compressive plastic macrostructural strains associated with macrostructural hardening. Small negative values of f_C are computed only at the very end of the path.

The final state of the sample is a denser macrostructure, with a net increment in the value of p_0^* and a larger elastic domain given by the final position of the yield surface LC_D.

4.2. Cyclic wetting/drying test

Two tests carried out by Pousada [22] have been selected to examine the response of an expansive clay subjected to suction cycles under oedometric conditions at two different vertical

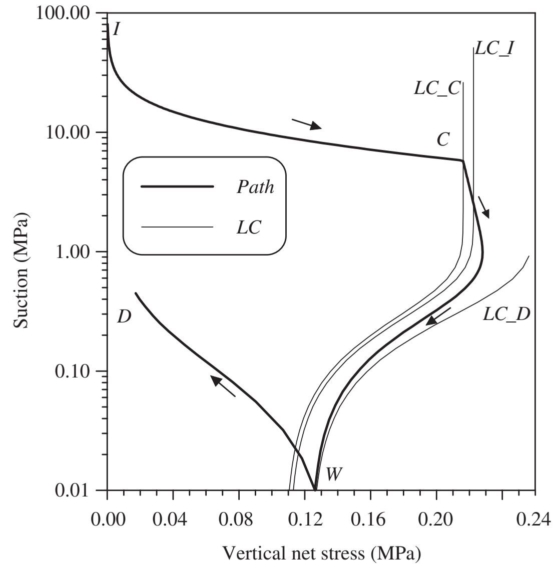

Figure 12. Computed stress path, together with the positions of the LC curve in the σ_v–s plane.

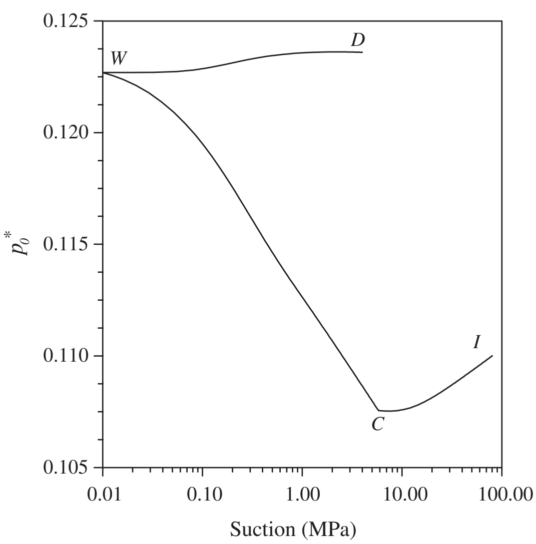

Figure 13. Evolution of the hardening parameter, p_0^*, during the test.

stress levels. The tests correspond to samples with a dry density of 1.34 mg/m^3 and with an initial water content of 24% that were subjected to six wetting–drying suction cycles with suction changing from 0.2 to 1.7 MPa and back. Table II shows the values of the parameters used to model the tests.

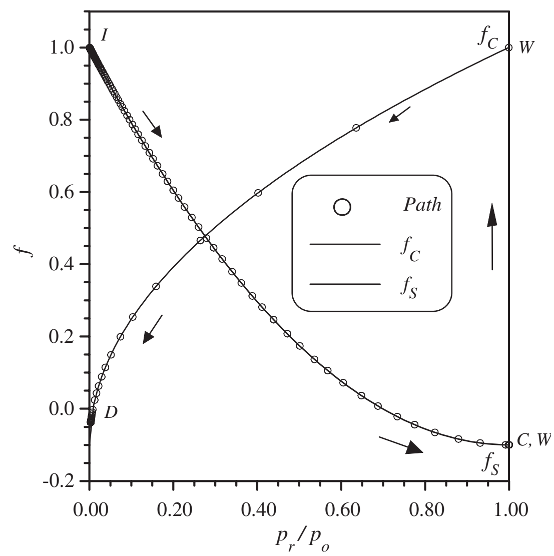

Figure 14. Evolution of the f_C and f_S interaction functions.

Table II. Parameters used to define the elasto-plastic constitutive law (Section 4.2).

Parameters defining the Barcelona basic model for macrostructural behaviour
$\kappa = 0.050$ $\kappa_s = 0.001$ $\lambda_{(0)} = 0.065$ p_c (MPa) $= 0.01$ $r = 0.96$ ζ (MPa^{-1}) $= 0.20$ p_0^* (MPa) $= 0.75$
Parameters defining the law for microstructural behaviour
α_m (MPa^{-1}) $= 8.0 \times 10^{-1}$ β_m (MPa^{-1}) $= 2.0 \times 10^{-2}$ $\chi = 1$
Interaction functions
$f_C = 1.6 + 0.6 \tanh(10(p_r/p_0) - 0.40)$; $f_S = 1.6 - 0.6 \tanh(10(p_r/p_0) - 0.40)$
$e_{macro} = 0.55$ $e_{micro} = 0.45$

The experimentally observed response of the material, in terms of volumetric deformations, at two different vertical stresses (0.01 and 0.1 MPa) is presented in Figures 15(a) and (b). These plots also show the results from the constitutive model in terms of: volumetric strains, macrovoid and microvoid ratio. It can be observed that the response obtained is good in qualitative terms. The model can reproduce the tendency to reduce the swelling capacity of the material when the vertical stress increases, both, in total strain values and in their irrecoverable components. The reductions in the accumulated strains, as cycles accumulate, are also well captured by the model in both tests. This type of behaviour can be explained considering double structure concepts.

Point E, in the interaction functions, corresponds to the equilibrium condition reached after a certain number of cycles when the suction cycles develop symmetric paths around it [14]. For both tests, the suction cycles develop predominantly on the left side of point E. This implies net expansions of the samples, which are more marked in the case of the small stress level. This is due to the fact that the initial stress is further away from point E in the case of the sample under

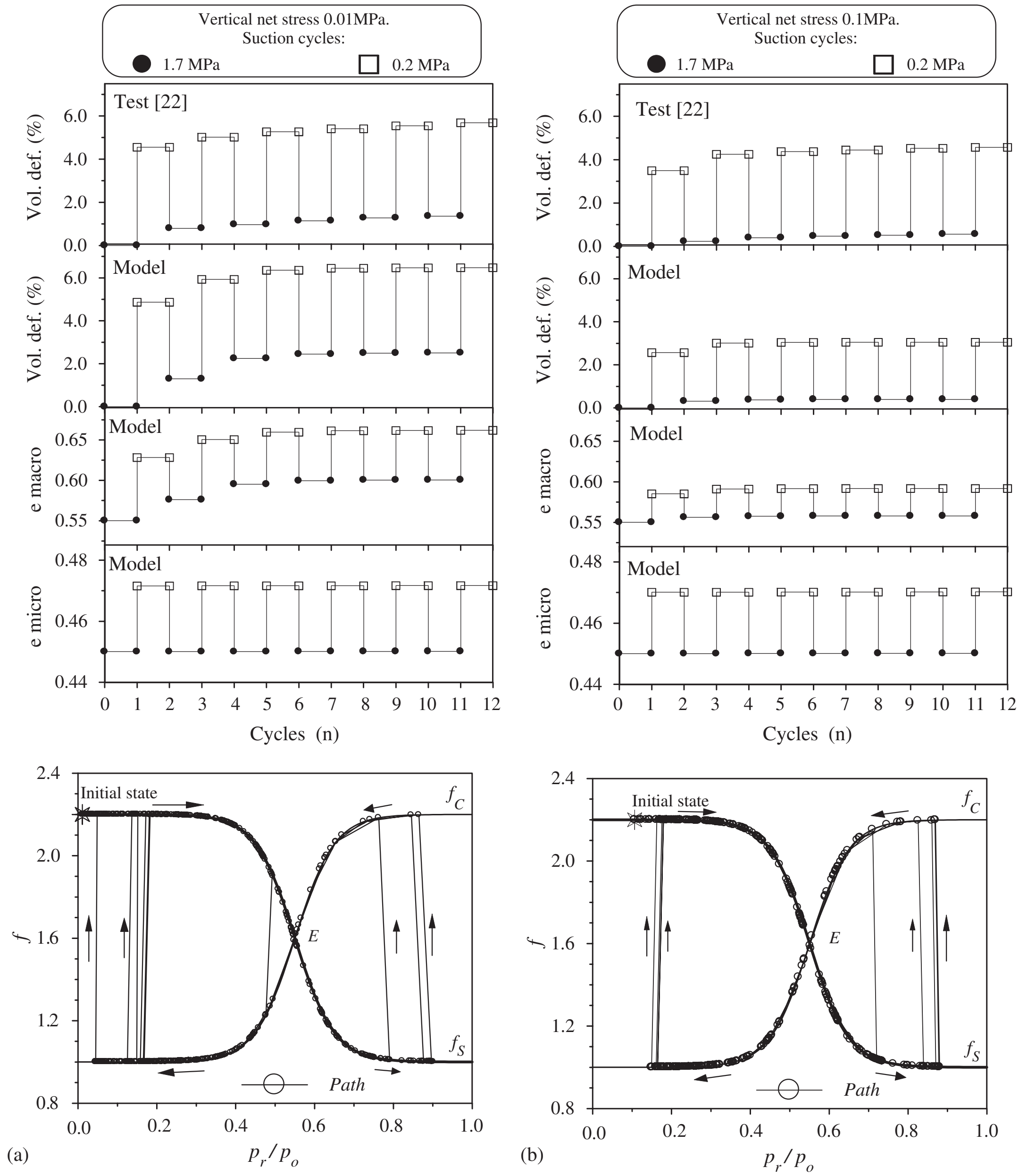

Figure 15. (a) $\sigma_v = 0.01$ MPa, (b) $\sigma_v = 0.1$ MPa. Values of volumetric deformations (reported and computed), macro- and microvoid ratios induced by suctions cycles (upper graph). Evolution of the interaction functions (lower graph).

the smaller stress implying larger macrostructural strains induced by the interaction mechanism. Another interesting aspect is the evolution of the micro- and macrovoid ratios as the cycles increase. The microstructural behaviour is reversible and the changes in the microstructural void ratio are not greatly affected by the stress level. On the other hand, the macrostructural void ratio is significantly influenced by the values of applied stress. This can be attributed to the increased difficulty of modifying the macrostructural arrangement when the material confinement is higher.

4.3. THM response of the FEBEX bentonite

4.3.1. Overheating episode. A difficulty in validating this type of models is the lack of experimental results involving complex THM stress paths. However, a large-scale heating test that is being carried out in CIEMAT (Madrid) [46], has provided relevant data to evaluate the performance of the model. The layout of the test is depicted in Figure 16. Two electrical heaters (simulating canisters containing heat-emitting waste) were placed in the centre of a steel cylinder 6 m long and with inner diameter of 1.62 m. The space between the heaters and the steel cylinder was filled with a 0.64 m thick engineered barrier made up of compacted bentonite. The barrier is hydrated uniformly from all around the cylinder with an applied water pressure of about 0.5 MPa. Simultaneously, the barrier was heated maintaining a constant temperature of 100°C at the contact between heaters and bentonite. The THM behaviour of the heating test has been successfully modelled [46, 47].

On day 1391 of the experiment an accidental overheating occurred. Figure 17 shows the evolution of temperatures at various radii in the barrier. It can be seen that points close to the heater reached temperatures in excess of 200°C (more than 100°C above the prescribed temperature). Afterwards the heaters were switched off and the barrier cooled down rapidly to temperatures close to 45°C near the heater. Finally, the prescribed thermal conditions of the test were re-established, i.e. a constant temperature of 100°C at the contact between heaters and clay. Figure 18 shows the evolution of suction for a point close to the heater. Firstly, the suction reduced from 110 to 55 MPa due to the passage of a vapour front. Afterwards, thermally

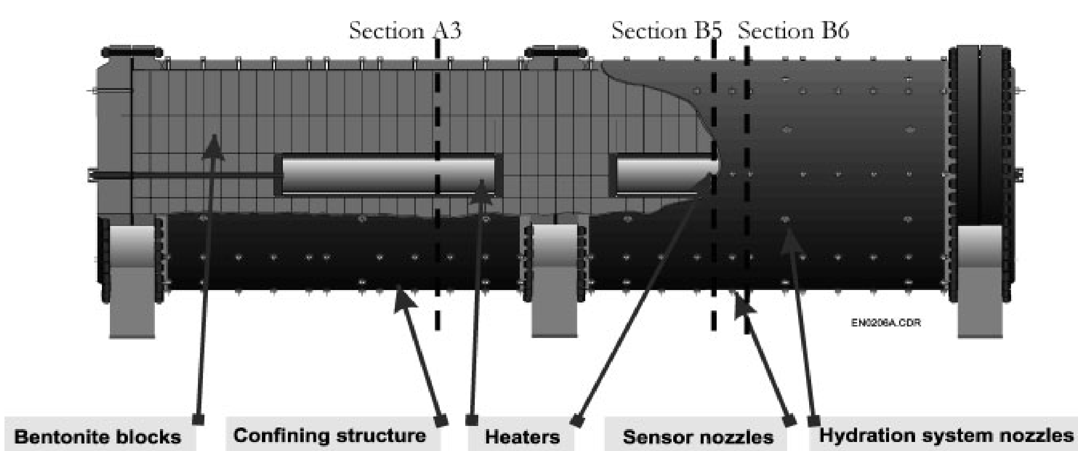

Figure 16. Layout of the large-scale heating test.

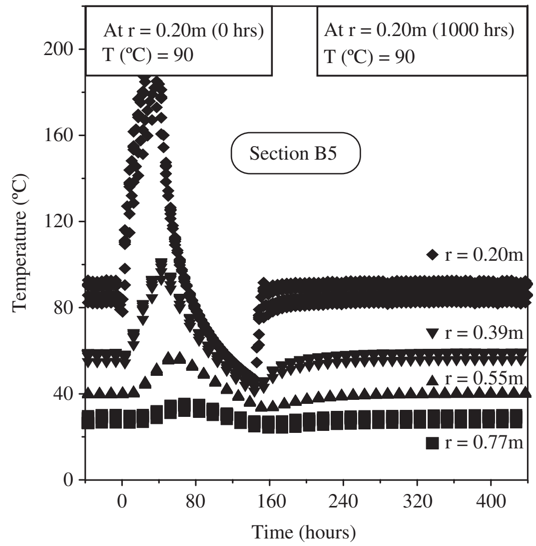

Figure 17. Evolution of temperature during and after the overheating event.

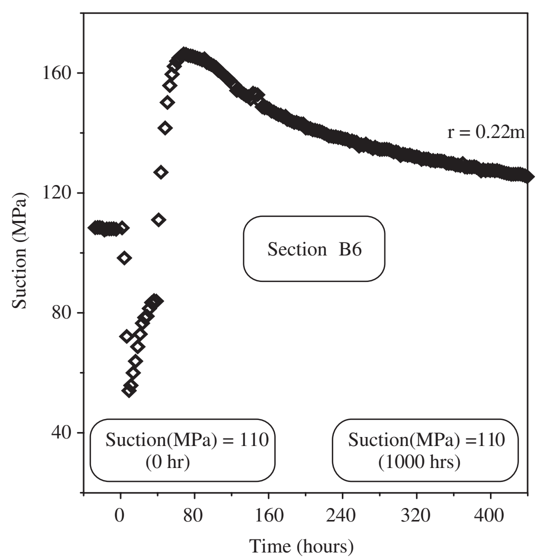

Figure 18. Evolution of suction during and after the overheating event.

induced drying increased the suction to values close to 165 MPa. Finally there was a tendency to recover the value before the event.

The evolution of the radial stress in the barrier is especially interesting. Figure 19 presents the evolution of radial stress in two representative sections of the barrier. Just after overheating,

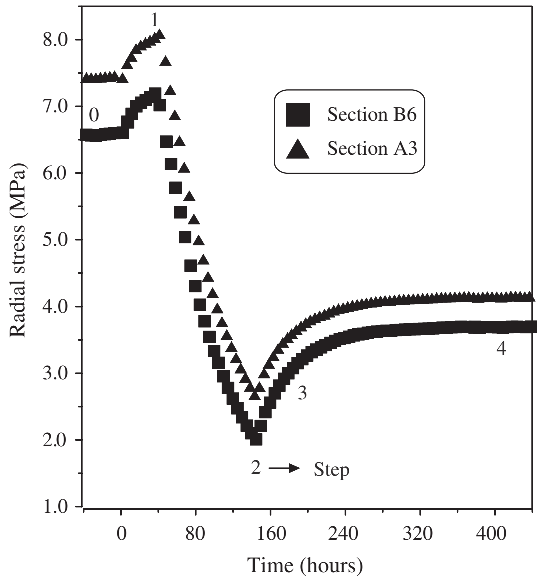

Figure 19. Evolution of radial stresses during and after the overheating event.

there was a moderate increase of radial stress followed by a strong reduction down to around 2 MPa. The radial stress recovered somewhat subsequently but it remained very far from the initial values. There was a large irreversible net reduction of radial stress. This behaviour was detected in all the sensors placed in sections involving heaters.

4.3.2. Overheating modelling. Herein it will be examined whether the mechanical model is consistent with the observations of irreversible phenomena indicated above. The following considerations should be pointed out: (i) only the constitutive law is tested so there are no time effects due to the transient phenomena occurring in the barrier, (ii) the information attributed to the constitutive law point corresponds in fact to a zone of the barrier of finite size, and (iii) the aim is not to reproduce the full behaviour of the barrier but to check whether the main features of the observed mechanical behaviour are a natural outcome of the constitutive model.

A synthetic generalized stress path was applied to the constitutive law, corresponding to four major episodes: a wetting due to the passage of a vapour front, an intense drying associated with the increase of temperature, a subsequent cooling due to the switching off of the heaters and, finally, the re-establishment of the prescribed test conditions. Table III summarizes the four main loading stages of the overheating episode.

Regarding model parameters, the laboratory work aimed at the THM characterization of the FEBEX bentonite has provided valuable information for this purpose. Two main types of tests have been used to validate the model: oedometric tests, in which a wide combination of generalized loading paths has been considered; and swelling pressure tests [47]. Table IV presents the values adopted for the model parameters.

Figures 20–22 show the model results when the loading stages indicated in Table III were applied. The suction and temperature changes were applied under conditions of no volume

Table III. Main loading stages of the overheating (average records).

Stage	Description	s (MPa)	T (°C)	σ_r (MPa)
0	Initial conditions before overheating	110	90	6.5–7.5
1	Reduction of suction (due to the vapour front passage) and increase of temperature, below the maximum value	55	135	7.5–8.0
2	Achievement of the maximum temperature and suction	165	200	2.0–2.5
3	Cooling down of the barrier to the minimum observed temperature	155	45	2.5–3.5
4	Re-establishment of the initial thermal and hydraulic conditions	110	90	3.5–4.0

Table IV. Parameters used to define the elasto-plastic constitutive law (Section 4.3).

Parameters defining the Barcelona basic model for macrostructural behaviour

$\kappa = 0.005 \quad \kappa_s = 0.001 \quad \lambda_{(0)} = 0.080 \quad p_c \text{ (MPa)} = 0.50$

$r = 0.90 \quad \zeta \text{ (MPa}^{-1}) = 1.00 \quad p_0^* \text{ (MPa)} = 6.5 \quad \alpha_0 \text{ (°C}^{-1}) = 1.0 \times 10^{-5}$

Parameters defining the law for microstructural behaviour

$\alpha_m \text{ (MPa}^{-1}) = 2.1 \times 10^{-6} \quad \beta_m \text{ (MPa}^{-1}) = 2.3 \times 10^{-5} \quad \chi = 1$

Interaction functions

$f_C = 1 + 0.9 \tanh(20(p_r/p_0) - 0.25); \quad f_S = 0.8 - 1.1 \tanh(20(p_r/p_0) - 0.25)$

$e_{macro} = 0.20 \qquad e_{micro} = 0.45$

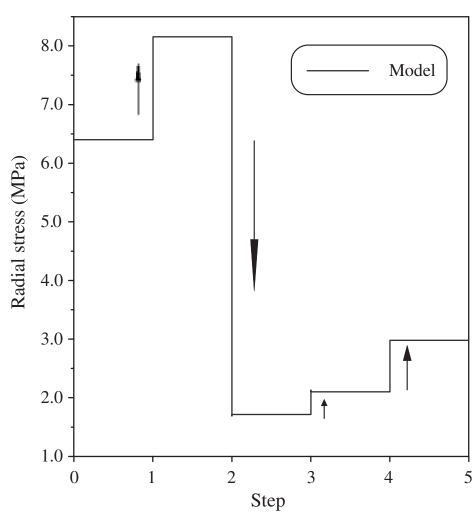

Figure 20. Computed values of radial stress during the application of the generalized stress path.

change, mimicking the confined state of the test. Therefore, zero strain in all directions and an isotropic stress state was assumed. Figure 23 shows a three-dimensional representation of the four loading stages.

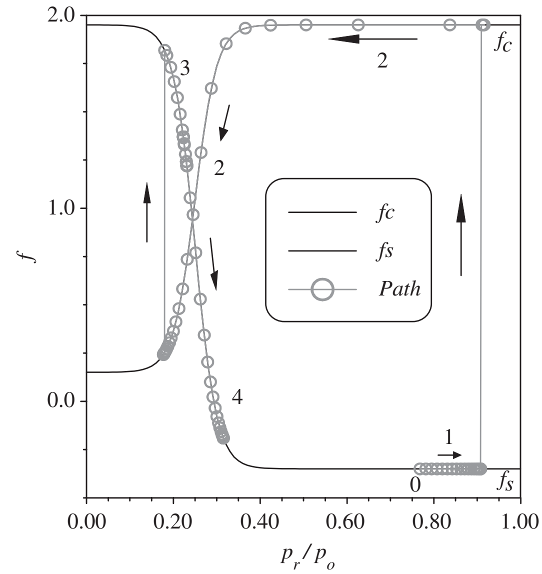

Figure 21. Evolution of the stress state on the f_C and f_S interaction functions.

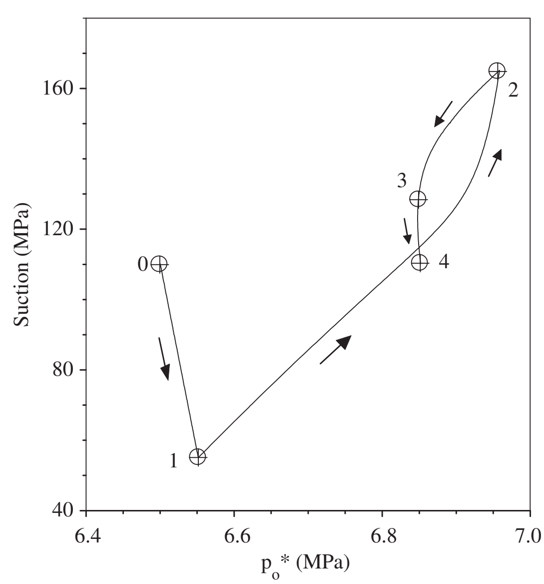

Figure 22. Evolution of the hardening parameter during the four loading stages.

A reasonable correspondence between measured and calculated values of radial pressure is observed (Figure 20). Figure 21 depicts the calculated evolution of the interaction functions and Figure 22 shows the evolution of the hardening parameter.

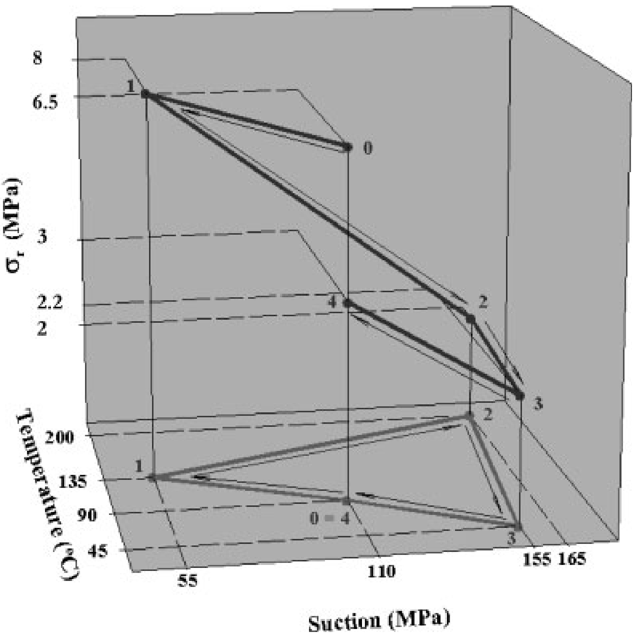

Figure 23. Three-dimensional representation of the applied generalized stress path.

In the first loading stage the elastic mechanisms associated with suction reduction and temperature increase tend to increase the swelling pressure because they are associated with soil expansion. In this path the interaction function f_S has negative values, which implies a hardening of the material. Heating continues in the second stage but now it is associated with a drying of the soil (increase of suction). This intense drying dominates and causes a tendency to contract and, consequently, a swelling pressure reduction occurs. During this stage (mc mechanism active) the interaction between the two structural levels produces a densification of the macrostructure. The third stage is characterized by a reduction of temperature and a wetting of the material; the latter dominates causing a tendency to expand and hence an increase of swelling pressure. At the final stage, the initial thermal and hydraulic variables are again prescribed, continuing the wetting of the material and increasing the temperature. These two factors lead to a tendency for expansion of the soil and hence an increase of swelling pressure. During the last two stages the ms mechanism is active. The interaction between the two structures causes an expansion of the macrostructure and a reduction of p_0^* during the main part or this path. This behaviour tends to change in the later part of this stage, when the stress path reaches negative values of the interaction function.

According to the model, the intense drying of stage 2 affects strongly the behaviour of the bentonite during this event, inducing changes in the clay structure that are not recovered when returning to the conditions before the overheating. The final outcome is that the constitutive model response to this complex THM generalized stress path is a significant reduction in swelling stress, the same behaviour as that observed in the heating test.

Naturally, this analysis does not reproduce exactly the conditions of the test, as it involves instantaneous application of the thermal and hydraulic loading without considering the transient phenomena that actually occurred in the barrier. It is therefore not surprising that there is a certain time lag between test observations and constitutive model predictions. In any case, the main objective of proving the capability of the model to reproduce irreversible behaviour when is submitted to complex THM loading paths has been largely achieved. Also a physical explanation has been suggested to explain the observed bentonite behaviour.

5. CONCLUSIONS

In order to represent more closely the typical fabric of expansive clays the mechanical model described in this paper considers the existence of two pores structures. The explicit inclusion in the constitutive law of these two basic structural levels, and their main interactions, provides a powerful approach to analyse and to describe the behaviour of expansive clays. For instance, the typical evolution of swelling strain or swelling pressure observed in expansive soils under wetting can be described by the integration in the model, at microstructural level, of simple laws based on clay minerals behaviour. Moreover, the inclusion of a suitable law for the macrostructure level allows characteristic phenomena that affect the global arrangements of clays aggregates to be reproduced, such as macrostructural collapse (i.e. Section 4.1). Finally, the consideration of the interaction between both structural levels plays a crucial role to explain complex behaviour features observed in expansive materials (i.e. Sections 4.2 and 4.3).

The constitutive law has been formulated in the context of elasto-plasticity for strain hardening materials. A well-known elasto-plastic model for unsaturated soils, which describes the macrostructural behaviour, has been combined with a generalized plasticity model to reproduce the irreversible effects related to the interaction between the two structural levels. The model has been implemented in the finite element program CODE_BRIGHT and has exhibited good performance when it has been applied to reproduce a number of experimental results involving expansive materials.

APPENDIX A

Figure A1 shows the phase diagram adopted and Equations (A1)–(A4) contain some of the variables used in this work.

$$V = V_{\mathrm{s}} + V_{v\mathrm{m}} + V_{v\mathrm{M}} = V_{\mathrm{m}} + V_{v\mathrm{M}} \tag{A1}$$

$$V_v = V_{v\mathrm{m}} + V_{v\mathrm{M}} \tag{A2}$$

$$e = \frac{V_v}{V_{\mathrm{s}}} = e_{\mathrm{M}} + e_{\mathrm{m}} = \frac{V_{v\mathrm{M}}}{V_{\mathrm{s}}} + \frac{V_{v\mathrm{m}}}{V_{\mathrm{s}}} \tag{A3}$$

$$\bar{e}_{\mathrm{m}} = e_{\mathrm{m}} = \frac{V_{v\mathrm{m}}}{V_{\mathrm{s}}} \tag{A4}$$

A more detailed explanation of the variables and laws related to the double structure approach can be found in Reference [20].

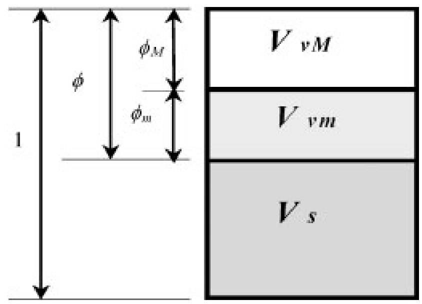

Figure A1. Phase diagram adopted.

APPENDIX B

A detailed description of the BBM model can be found in References [21, 41], here the more relevant equations used in this work are presented. Equation (1) is expressed in terms of stress invariants defined as

$$p = \tfrac{1}{3}(\sigma_x + \sigma_y + \sigma_z) \tag{B1}$$

$$J^2 = 0.5 \text{ trace}(\mathbf{s}^2) \tag{B2}$$

$$\theta = -\tfrac{1}{3}\sin^{-1}(1.5\sqrt{3}\det \mathrm{s}/J^3) \tag{B3}$$

$$\mathbf{s} = \boldsymbol{\sigma} - p\mathbf{I} \tag{B4}$$

$$\boldsymbol{\sigma} = \boldsymbol{\sigma}_{\mathrm{t}} - \mathbf{I}p_{\mathrm{f}} \tag{B5}$$

where

$$p_{\mathrm{f}} = p_{\mathrm{g}} \quad \text{if } p_{\mathrm{g}} > p_{\mathrm{l}} \quad \text{otherwise } p_{\mathrm{f}} = p_{\mathrm{l}}$$

I is the identity tensor.

The following equations are related to Equation (1):

$$p_{\mathrm{s}} = ks\,\mathrm{e}^{-\rho\Delta T} \tag{B6}$$

p_{s} considers the dependence of shear stress on suction and temperature. k and ρ are model parameters. The equation that defines the set of yield p_0 values for each associated suction is given by

$$p_0 = p_c\left(\frac{p_{0T}^*}{p_c}\right)^{(\lambda_{(0)}-\kappa)/(\lambda_{(\mathrm{s})}-\kappa)} \tag{B7}$$

where p_c is a reference stress, κ is the elastic stiffness parameter for changes in net mean stress, p_{0T}^* is the pre-consolidation net mean stress for saturated conditions at current temperature. $\lambda_{(\mathrm{s})}$ is the compressibility parameter for changes in net mean stress for virgin states of the soil, which depends on suction according to

$$\lambda_{(s)} = \lambda_{(0)}[r + (1 - r)\mathrm{e}^{-\zeta s}] \tag{B8}$$

where r is a parameter which defines the minimum soil compressibility (at infinity suction) and ζ is a parameter which controls the rate of decrease of soil compressibility with macrostructural suction.

According to Reference [41], p^*_{0T} can be expressed as

$$p^*_{0T} = p^*_0 + 2(\alpha_1 \Delta T + \alpha_3 \Delta T|\Delta T|) \tag{B9}$$

where α_1 and α_3 are material parameters.

Finally, the normal to the yield surface is defined as

$$\mathbf{n}_{\mathrm{LC}} = \frac{\partial F_{\mathrm{LC}}}{\partial \boldsymbol{\sigma}} \tag{B10}$$

APPENDIX C: ELASTIC MODEL

In this section the elastic tensors for the general case are presented. More details can be found in Reference [45]. The elastic matrix is evaluated as follows:

$$\mathbf{D}_{\mathrm{e}} = \begin{bmatrix} K + \frac{4}{3}G_t & K - \frac{2}{3}G_t & K - \frac{2}{3}G_t & 0 & 0 & 0 \\ & K + \frac{4}{3}G_t & K - \frac{2}{3}G_t & 0 & 0 & 0 \\ & & K + \frac{4}{3}G_t & 0 & 0 & 0 \\ & & & G_t & 0 & 0 \\ \text{symm} & & & & G_t & 0 \\ & & & & & G_t \end{bmatrix} \tag{C1}$$

where K is the global bulk modulus and G_t is the shear modulus. K may be computed considering the elastic contribution of the two pores structures, the global stiffness is defined as

$$K = \left(\frac{1}{K_{\mathrm{M}}} + \frac{1}{K_{\mathrm{m}}}\right)^{-1} \tag{C2}$$

where K_{M} is the macrostructural bulk modulus for changes in mean stress, computed as

$$K_{\mathrm{M}} = \frac{(1 + e_{\mathrm{M}})}{\kappa} p \tag{C3}$$

For the microstructural bulk modulus (K_{m}) the following two laws have been implemented [42]:

$$K_{\mathrm{m}} = \frac{\mathrm{e}^{-\alpha_{\mathrm{m}}\hat{p}}}{\beta_{\mathrm{m}}} \tag{C4a}$$

$$K_{\mathrm{m}} = \frac{(1 + \bar{e}_{\mathrm{m}})}{\kappa_{\mathrm{m}}} \hat{p} \tag{C4b}$$

The macrostructural bulk modulus for changes in suction has been computed considering the following law [45]:

$$K_s = \frac{(1 + e_M)(s + p_{at})}{\kappa_s} \tag{C5}$$

Finally, the macrostructural bulk modulus for changes in temperature is evaluated through the expression [41]:

$$K_T = \frac{1}{(\alpha_0 + \alpha_2 \Delta T)} \tag{C6}$$

APPENDIX D

At the image point projection it is assumed that η, θ, s and T are maintained constant during projection. The following equations define the projection:

$$p^{\otimes} = \frac{[g(\theta)/[g(-30^{\circ})]]^2 M^2 p_0 - \eta^2 p_s}{[g(\theta)/[g(-30^{\circ})]]^2 M^2 + \eta^2}, \quad J^{\otimes} = \frac{1}{\sqrt{3}} \eta (p^{\otimes} + p_s) \tag{D1}$$

where

$$\eta = \frac{\sqrt{3} J}{p + p_s} = \frac{\sqrt{3} J^{\otimes}}{p^{\otimes} + p_s} \tag{D2}$$

with $s^{\otimes} = s$, $\theta^{\otimes} = \theta$ and $T^{\otimes} = T$.

Regarding the direction of the plastic strain increment (related to this plastic mechanism) a non-associated flow rule in the plane $s = \text{constant}$ and $T = \text{constant}$ is suggested. This is a similar assumption as the one made for the BBM by Alonso *et al.* [21] and Gens [41].

The components of the normal to the plastic potential at the image point (17) are defined as

$$\frac{\partial G}{\partial p^{\otimes}} = \left[\frac{g(\theta)}{g(-30^{\circ})}\right]^2 M^2 (2p^{\otimes} + p_s - p_0) \tag{D3}$$

$$\frac{\partial G}{\partial J^{\otimes}} = 6\alpha J^{\otimes} \tag{D4}$$

$$\frac{\partial G}{\partial \theta^{\otimes}} = -\frac{2g(\theta)g'(\theta)}{[g(-30^{\circ})]^2} M^2 (p^{\otimes} + p_s)(p_0 - p^{\otimes}) \tag{D5}$$

APPENDIX E

E.1. Auxiliary expressions for the macrostructural model

The consistency condition can be expressed as

$$\dot{F}_{LC} = 0 = \mathbf{n}_{LC} \cdot \dot{\boldsymbol{\sigma}} + l_{LC}\dot{s} + d\dot{T} + \bar{H}(\dot{\boldsymbol{\varepsilon}}^{p}_{vLC} + \dot{\boldsymbol{\varepsilon}}^{p}_{v\beta}) \tag{E1}$$

where

$$l_{\mathrm{LC}} = \frac{\partial F_{\mathrm{LC}}}{\partial s} \tag{E2}$$

$$d = \frac{\partial F_{\mathrm{LC}}}{\partial T} \tag{E3}$$

$$\bar{H} = \frac{\partial F_{\mathrm{LC}}}{\partial p_0} \frac{\partial p_0}{\partial p_0^*} \frac{\partial p_0^*}{\partial \varepsilon_v^{\mathrm{p}}} \tag{E4}$$

$$\dot{\varepsilon}_{v\mathrm{LC}}^{\mathrm{p}} = \dot{\lambda}_{\mathrm{LC}} \mathbf{m}^{\mathrm{T}} \cdot \mathbf{m}_{\mathrm{LC}} \tag{E5}$$

$$\dot{\varepsilon}_{v\beta}^{\mathrm{p}} = \dot{\lambda}_{\beta} \mathbf{m}^{\mathrm{T}} \cdot \mathbf{m}_{\beta} \tag{E6}$$

The net stress increment can be expressed as

$$\dot{\boldsymbol{\sigma}} = \mathbf{D}_{\mathrm{e}} \cdot (\dot{\boldsymbol{\varepsilon}} - \dot{\boldsymbol{\varepsilon}}_{\mathrm{s}}^{\mathrm{e}} - \dot{\boldsymbol{\varepsilon}}_{\mathrm{T}}^{\mathrm{e}} - \dot{\boldsymbol{\varepsilon}}_{\mathrm{LC}}^{\mathrm{p}} - \dot{\boldsymbol{\varepsilon}}_{\beta}^{\mathrm{p}}) = \mathbf{D}_{\mathrm{e}} \cdot (\dot{\boldsymbol{\varepsilon}} - b\mathbf{m}\dot{s} - c\mathbf{m}\dot{T} - \dot{\lambda}_{\mathrm{LC}} \mathbf{m}_{\mathrm{LC}} - \dot{\lambda}_{\beta} \mathbf{m}_{\beta}) \tag{E7}$$

After some algebra on (E1) and (E7) [20] Equation (32) is obtained, where

$$\bar{H}_{\mathrm{LC}} = H_{\mathrm{LC}} + H_{\mathrm{LC}}^{\mathrm{c}} = H_{\mathrm{LC}} + \mathbf{n}_{\mathrm{LC}}^{\mathrm{T}} \cdot \mathbf{D}_{\mathrm{e}} \cdot \mathbf{m}_{\mathrm{LC}} \tag{E8}$$

$$\bar{h}_{\beta} = h_{\beta} + h_{\beta}^{\mathrm{c}} = h_{\beta} + \mathbf{n}_{\mathrm{LC}}^{\mathrm{T}} \cdot \mathbf{D}_{\mathrm{e}} \cdot \mathbf{m}_{\beta} \tag{E9}$$

$$\dot{e}_{\mathrm{LC}} = \mathbf{n}_{\mathrm{LC}}^{\mathrm{T}} \cdot \mathbf{D}_{\mathrm{e}} \cdot \dot{\boldsymbol{\varepsilon}} \tag{E10}$$

$$\dot{s}_{\mathrm{LC}} = [l_{\mathrm{LC}} + l_{\beta} + \mathbf{n}_{\mathrm{LC}}^{\mathrm{T}} \cdot (\boldsymbol{\alpha}_{\mathrm{s}} + \boldsymbol{\beta}_{\mathrm{s}})]\dot{s} \tag{E11}$$

$$\dot{t}_{\mathrm{LC}} = (d + \mathbf{n}_{\mathrm{LC}}^{\mathrm{T}} \cdot \boldsymbol{\alpha}_T)\dot{T} \tag{E12}$$

$$\boldsymbol{\alpha}_{\mathrm{s}} = -b\mathbf{D}_{\mathrm{e}} \cdot \mathbf{m} = \left(\frac{1}{K_{\mathrm{s}}} + \frac{\chi}{K_{\mathrm{m}}}\right)\mathbf{D}_{\mathrm{e}} \cdot \mathbf{m} \tag{E13}$$

$$\boldsymbol{\beta}_{\mathrm{s}} = -\frac{1}{H_{\beta}} \omega_{\beta} \chi \mathbf{D}_{\mathrm{e}} \cdot \mathbf{m}_{\beta} \tag{E14}$$

$$\boldsymbol{\alpha}_T = c\mathbf{D}_{\mathrm{e}} \cdot \mathbf{m} = \frac{1}{K_T} \mathbf{D}_{\mathrm{e}} \cdot \mathbf{m} \tag{E15}$$

$$H_{\mathrm{LC}} = -\bar{H}\mathbf{m}^{\mathrm{T}} \cdot \mathbf{m}_{\mathrm{LC}} \tag{E16}$$

$$h_{\beta} = -\bar{H}\mathbf{m}^{\mathrm{T}} \cdot \mathbf{m}_{\beta} \tag{E17}$$

$$l_{\beta} = -\frac{1}{H_{\beta}} h_{\beta} \omega_{\beta} \chi \tag{E18}$$

E.2. Auxiliary expressions for the generalized plasticity model. For the generalized plasticity model, a procedure similar to the one suggested by Pastor *et al.* [29] has been followed. Firstly, a decomposition of strain increment is assumed:

$$\dot{\boldsymbol{\varepsilon}} = \dot{\boldsymbol{\varepsilon}}^{\mathrm{e}} + \dot{\boldsymbol{\varepsilon}}^{\mathrm{p}}_{\mathrm{LC}} + \dot{\boldsymbol{\varepsilon}}^{\mathrm{p}}_{\beta} \tag{E19}$$

Then, pre-multiplying (E19) by $\mathbf{n}_\beta^{\mathrm{T}}\mathbf{D}_{\mathrm{e}}$ and operating, it gives

$$\begin{aligned}\mathbf{n}_\beta^{\mathrm{T}} \cdot \mathbf{D}_{\mathrm{e}} \cdot \dot{\boldsymbol{\varepsilon}} = \mathbf{n}_\beta^{\mathrm{T}} \cdot \dot{\boldsymbol{\sigma}} + b\mathbf{n}_\beta^{\mathrm{T}} \cdot \mathbf{D}_{\mathrm{e}} \cdot \mathbf{m}\dot{s} + c\mathbf{n}_\beta^{\mathrm{T}} \cdot \mathbf{D}_{\mathrm{e}} \cdot \mathbf{m}\dot{T} + \frac{\chi}{H_\beta}\omega_\beta \mathbf{n}_\beta^{\mathrm{T}} \cdot \mathbf{D}_{\mathrm{e}} \cdot \mathbf{m}_\beta \dot{s}\\ + \dot{\lambda}_\beta \mathbf{n}_\beta^{\mathrm{T}} \cdot \mathbf{D}_{\mathrm{e}} \cdot \mathbf{m}_\beta + \dot{\lambda}_{\mathrm{LC}} \mathbf{n}_\beta^{\mathrm{T}} \cdot \mathbf{D}_{\mathrm{e}} \cdot \mathbf{m}_{\mathrm{LC}}\end{aligned} \tag{E20}$$

After some algebra on (E7) and (E20) [20] Equation (33) is obtained, where

$$\bar{h}_{\mathrm{LC}} = h^{\mathrm{c}}_{\mathrm{LC}} = \mathbf{n}_\beta^{\mathrm{T}} \cdot \mathbf{D}_{\mathrm{e}} \cdot \mathbf{m}_{\mathrm{LC}} \tag{E21}$$

$$\bar{H}_\beta = H_\beta + H^{\mathrm{c}}_\beta = H_\beta + \mathbf{n}_\beta^{\mathrm{T}} \cdot \mathbf{D}_{\mathrm{e}} \cdot \mathbf{m}_\beta \tag{E22}$$

$$\dot{e}_\beta = \mathbf{n}_\beta^{\mathrm{T}} \cdot \mathbf{D}_{\mathrm{e}} \cdot \dot{\boldsymbol{\varepsilon}} \tag{E23}$$

$$\dot{s}_\beta = \mathbf{n}_\beta^{\mathrm{T}} \cdot (\boldsymbol{\alpha}_{\mathrm{s}} + \boldsymbol{\beta}_{\mathrm{s}})\dot{s} \tag{E24}$$

$$\dot{t}_\beta = \mathbf{n}_\beta^{\mathrm{T}} \cdot \boldsymbol{\alpha}_T \dot{T} \tag{E25}$$

APPENDIX F

In this appendix, with the objective of completeness, some algebra notions on *P-matrix* given in Reference [18] have been transcribed.

Definition

- The 'principal sub-matrix' $\mathbf{A}_\alpha$ of matrix $\mathbf{A} \in \mathscr{R}_{n\times n}$, is the matrix whose entries lie in rows and columns of $\mathbf{A}$ indexed by sets $\alpha \subseteq \{1, 2, \ldots, n\}$ (i.e. $\mathbf{A}_\alpha$ is a sub-matrix of $\mathbf{A}$ whose diagonal is part of the diagonal of $\mathbf{A}$). The determinant of $\mathbf{A}_\alpha$ is called a 'principal minor' of $\mathbf{A}$.
- The matrix $\mathbf{A} \in \mathscr{R}_{n\times n}$, 'reverse the sign' of the vector $\mathbf{X} = 0 \in \mathscr{R}^n$ if:

$$\mathbf{x}_i(\mathbf{A} \cdot \mathbf{X})_i \leqslant 0 \quad \forall i = 1, 2, \ldots, n$$

Definition

- A matrix $\mathbf{A} \in \mathscr{R}_{n\times n}$, is said to be a *P-matrix* when all its principal minors are positive. Let $\mathbf{A}$ $\mathscr{R}_{n\times n}$. The following statements are equivalent:

(a) **A** is a *P-matrix*.
(b) **A** does not reverse the sign of any vector, except the zero vector,

$$\text{i.e. } \mathbf{x}_i(\mathbf{A}\cdot\mathbf{X})_i \leqslant 0 \quad \forall i = 1, 2, \ldots, n \quad \text{implies } \mathbf{X} = 0$$

(c) All real eigenvalues of **A** and its principal sub-matrices are positive.

APPENDIX G: NOMENCLATURE

$\mathbf{D}_e$	elastic matrix
$\mathbf{D}_{ep}$	elasto-plastic matrix
e	void ratio
e_M	macrostructural level void ratio
e_m	microstructural level void ratio
f_β	interaction function for β mechanism
F_{LC}	BBM yield surface
F_{NL}	neutral line
g	Lode's angle function
G	plastic potential
G_t	shear modulus
$\mathbf{H}$	hardening modulus matrix
$\mathbf{H}^c$	critical softening matrix
$\bar{\mathbf{H}}$	effective hardening matrix
$\mathbf{I}$	identity matrix
J	2nd stress invariant of deviatoric stress tensor
k	parameter describing the increase in cohesion with suction
K	global bulk modulus
K_m	microstructural bulk modulus for changes in mean stress plus suction
K_M	macrostructural bulk modulus for changes in mean stress
K_s	macrostructural bulk modulus for changes in suction
K_T	macrostructural bulk modulus for changes in temperature
lc	plastic mechanism related to BBM
LC	loading–collapse yield surface (BBM)
$\mathbf{m}$	auxiliary unit vector $\mathbf{m}^T = (1, 1, 1, 0, 0, 0)$
$\mathbf{m}_{LC}$	flow rule direction of BBM
$\mathbf{m}_\beta$	flow rule direction of mechanism β
mc	plastic mechanism related to MC path
ms	plastic mechanism related to MS path
M	slope of critical state line
MC	microstructural contraction path
MS	microstructural swelling path
$\hat{p}$	microstructural effective stress
p	mean net stress
p_c	reference stress
p_r	reference stress

p_0	net mean yield stress at current suction and temperature
p_0^*	net mean yield stress for saturated conditions at reference temperature
p_{0T}^*	net mean yield stress for saturated conditions at current temperature
r	parameter defining the minimum macrostructural soil compressibility
s	matric suction $(p_{\mathrm{g}} - p_{\mathrm{l}})$
s_{o}	osmotic suction
s_{t}	total suction
T	temperature (T_0 = reference temperature)
V, V_v	volume, volume of pores
V_{s}	volume of solids
$V_{v\mathrm{M}}, V_{v\mathrm{m}}$	V_v of macrostructure and microstructure

Greek letters

$\boldsymbol{\alpha}_{\mathrm{s}}$	elastic vector associated with suction
$\boldsymbol{\alpha}_{\mathrm{T}}$	elastic vector associated with temperature
α	parameter related to the plastic potential
α_0	parameter for elastic thermal strain
α_1	parameter that relates p_0^* with T
α_2	parameter for elastic thermal strain
α_3	parameter that relates p_0^* with T
α_{m}	parameter controlling the microstructural soil stiffness
$\boldsymbol{\beta}_{\mathrm{s}}$	elasto-plastic vector associated with suction
β	indicates the direction of the microstructural stress path ($\beta = C =>$ MC path, $\beta = S =>$ MS path)
β_{m}	parameter controlling the microstructural soil stiffness
γ_{s}	elasto-plastic vector associated with suction
γ_T	elasto-plastic vector associated with temperature
ΔT	temperature increment $(T - T_0)$
$\boldsymbol{\varepsilon}$	strain vector $\varepsilon_x, \varepsilon_y, \varepsilon_z, \gamma_{xy}, \gamma_{xz,}\gamma_{yz}{}^{\mathrm{T}}$
$\dot{\boldsymbol{\varepsilon}}^{\mathrm{e}}$	elastic strain increment due to stress changes
$\dot{\boldsymbol{\varepsilon}}_{\mathrm{s}}^{\mathrm{e}}$	elastic strain increment due to suction changes
$\dot{\boldsymbol{\varepsilon}}_T^{\mathrm{e}}$	elastic strain increment due to temperature changes
$\varepsilon_{v\mathrm{m}}$	elastic volumetric strain at microstructural level
$\varepsilon_v^{\mathrm{p}}$	total plastic volumetric strain
$\varepsilon_{vi}^{\mathrm{p}}$	plastic volumetric strain related to i plastic mechanism ($i = \mathrm{lc}, \beta$)
ζ	parameter controlling the rate of increase of macrostructural soils stiffness with suction
η	stress ratio
θ	Lode's angle
κ	macrostructural elastic stiffness parameter for changes in mean stress
κ_{s}	macrostructural elastic stiffness parameter for changes in suction
κ_{m}	parameter controlling the microstructural soil stiffness
$\lambda_{(\mathrm{s})}$	macrostructural compressibility parameter for changes in net mean stress for virgin states of soil at suction s
ρ	parameter that relates cohesion and T
$\boldsymbol{\sigma}_{\mathrm{t}}$	total stress vector $\sigma_x, \sigma_y, \sigma_z, \tau_{xy}, \tau_{xz}, \tau_{yz}{}_{\mathrm{t}}^{\mathrm{T}}$

$\boldsymbol{\sigma}$	net stress vector ($\boldsymbol{\sigma}_t - \mathbf{I}p_g$)
$\boldsymbol{\sigma}^*$	stress vector at the image point
$\hat{\boldsymbol{\sigma}}$	generalized stress vector
χ	F_{NL} slope
ω_β	variable related to β mechanism (= +1 for MC path, or = −1 for MS path)

ACKNOWLEDGEMENTS

The authors would like to acknowledge ENRESA for funding this work. The project FEBEX is partially funded by the European Commission. The authors are also grateful for the financial support given by CAPES (Coordenação de Aperfeiçoamento de Pessoal de Nível Superior, Brazil) and by the Ministerio de Ciencia y Tecnología of Spain through research grant BTE2001-2227.

REFERENCES

1. Bernier F, Volckaert G, Alonso EE, Villar M. Suction-controlled experiments on Boom clay. *Engineering Geology* 1997; **47**:325–338.
2. Al-Mukhtar M, Qi Y, Alcover JF, Bergaya F. Oedometric and water-retention behavior of highly compacted unsaturated smectites. *Canadian Geotechnical Journal* 1999; **36**:675–684.
3. Villar MV. Investigation of the behaviour of bentonite by means of suction-controlled oedometer tests. *Engineering Geology* 1999; **54**:67–73.
4. Komine A, Ogata N. Experimental study on swelling characteristics of compacted bentonite. *Canadian Geotechnical Journal* 1994; **31**:478–490.
5. Marcial D, Delage P, Cui YJ. On the high stress compression of bentonites. *Canadian Geotechnical Journal* 2002; **39**:812–820.
6. Lloret A, Villar MV, Sánchez M, Gens A, Pintado X, Alonso EE. Mechanical behaviour of heavily compacted bentonite under high suction changes. *Géotechnique* 2003; **53**(1):27–40.
7. Wiebe B, Graham J, Tang GX, Dixon D. Influence of pressure, saturation, and temperature on the behaviour of unsaturated sand-bentonite. *Canadian Geotechnical Journal* 1998; **35**:194–205.
8. Romero E. Characterisation and thermal-hydro-mechanical behaviour of unsaturated Boom clay: an experimental study. *Ph.D. Thesis*, Technical University of Catalonia, Spain, 1999.
9. Villar MV. Thermo-hydro-mechanical characterization of Cabo de Gata Bentonite. *Ph.D. Thesis*, Complutense University, Madrid, 2000 (in Spanish).
10. Sultan N, Delage P, Cui Y. Temperature effects on the volume change behaviour of Boom clay. *Engineering Geology* 2002; **64**:135–145.
11. Romero E, Gens A, Lloret A. Suction effects on a compacted clay under non-isothermal conditions. *Géotechnique* 2003; **53**(1):65–81.
12. Villar MV, Lloret A. Temperature influence on the hydro-mechanical behaviour of a compacted bentonite. *Workshop on Large Scale Field Tests in Granite*, Sitges, Spain, 2003 (CD format).
13. Gens A, Alonso EE. A framework for the behaviour of unsaturated expansive clays. *Canadian Geotechnical Journal* 1992; **29**:1013–1032.
14. Alonso E, Vaunat J, Gens A. Modelling the mechanical behaviour of expansive clays. *Engineering Geology* 1999; **54**:173–183.
15. Cui Y, Yahia-Aissa M, Delage P. A model for the volume change behaviour of heavily compacted swelling clays. *Engineering Geology* 2002; **64**:233–250.
16. Push R. Mineral water-interaction and their influence on the physical behaviour of highly compacted Na bentonite. *Canadian Geotechnical Journal* 1982; **19**:381–387.
17. Cui Y, Loiseau C, Delage P. Microstructure changes of a confined swelling soil due to suction controlled hydration. *Proceedings of the 3rd International Conference on Unsaturated Soils*, Recife, vol. 2, 2002; 593–598.
18. Rizzi E, Giulio M, Willam K. On failure indicators in multi-dissipative materials. *International Journal of Solids and Structures* 1996; **33**(20–22):3187–3214.
19. Olivella S, Gens A, Carrera J, Alonso EE. Numerical formulation for a simulator (CODE-BRIGHT) for the coupled analysis of saline media. *Engineering Computations* 1996; **13**(7):87–112.
20. Sánchez M. Thermo-hydro-mechanical coupled analyses in low permeability media. *Ph.D. Thesis*, Universitat Politécnica de Catalunya, Spain, July 2004.

21. Alonso E, Gens A, Josa A. A constitutive model for partially saturated soils. *Géotechnique* 1990; **40**(3):405–430.
22. Pousada PE. Deformabilidad de arcillas expansivas bajo succión controlada. *Ph.D. Thesis*, Technical University of Madrid, Spain, 1984.
23. Day RW. Swell-shrink behaviour of compacted clay. *Journal of Geotechnical Engineering* (ASCE) 1994; **120**(3): 618–623.
24. Subba Rao KS, Styadas G. Swelling potential with cycles of swelling and partial shrinkage. *Proceedings of the 6th International Conference on Expansive Soils*, New Delhi, vol. 1, 1987; 137–142.
25. Dif A, Bluemel F. Expansive soil under cyclic drying and wetting. *Geotechnical Testing Journal* 1991; **14**(1):96–102.
26. Al-Homoud S, Basma A, Malkawi H, Bashabsheh A. Cyclic swelling behaviour of clays. *Journal of Geotechnical Engineering* (ASCE) 1995; **121**(7):562–565.
27. Tripathy S, Subba K, Fredlund D. Water content-void ratio swell-shrink paths of compacted expansive soils. *Canadian Geotechnical Journal* 2002; **39**:938–959.
28 Zienkiewicz O, Leung A, Pastor M. Simple model for transient soil loading in earthquake analysis. I. Basic model and its application. *International Journal for Numerical and Analytical Methods in Geomechanics* 1985; **9**:453–476.
29 Pastor M, Zienkiewicz O, Chan A. Generalized plasticity and the modelling of soil behaviour. *International Journal for Numerical and Analytical Methods in Geomechanics* 1990; **14**:151–190.
30. Lubliner J, Auricchio F. Generalized plasticity and shape-memory alloys. *International Journal of Solids and Structures* 1996; **33**(7):991–1003.
31. Simoni L, Schrefler A. Parameter identification for suction-dependent plasticity model. *International Journal for Numerical and Analytical Methods in Geomechanics* 2001; **25**:273–288.
32. Lubliner J. A simple model of generalized plasticity. *International Journal of Solids and Structures* 1991; **28**(6): 769–778.
33. Guimaraes L, Gens A, Sánchez M, Olivella S. Chemo-mechanical modelling of expansive materials. *6th International Workshop on Key Issues in Waste Isolation Research*, Paris, 2001.
34. Guimarães LN. Análisis multi-componente no isotermo en medio poroso deformable no saturado. *Ph.D. Thesis*, Geotechnical Engineering Department, Technical University of Catalunya, Spain, 2002.
35. Lubliner J, Taylor R, Auricchio F. A new model of generalized plasticity and its numerical implementation. *International Journal of Solids and Structures* 1993; **30**(22):3171–3184.
36. Hueckel T, Baldi G. Thermoplasticity of saturated clays: experimental constitutive study. *Journal of Geotechnical Engineering* (ASCE) 1990; **116**(12):1778–1795.
37. Hueckel T, Borsetto M. Thermoplasticity of saturated soils and shales: constitutive equations. *Journal of Geotechnical Engineering* (ASCE) 1990; **116**(12):1765–1777.
38. Modaressi H, Laloui L. A thermo-viscoplastic constitutive model for clays. *International Journal for Numerical and Analytical Methods in Geomechanics* 1997; **21**:313–335.
39. Graham J, Tanaka N, Crilly T, Alfaro M. Modified cam-clay modelling of temperature effects in clays. *Canadian Geotechnical Journal* 2001; **38**:608–621.
40. Laloui L, Cekerevac C. Thermo-plasticity of clays: an isotropic yield mechanism. *Computer and Geotechnics* 2003; **30**:649–660.
41. Gens A. Constitutive laws. *Modern Issues in Non-saturated Soils*. Springer: Berlin, 1995; 129–158.
42. Alonso E. Modelling expansive soil behaviour. *Second International Conference on Unsatured Soils*, Beijing, vol. 1, 1998; 37–70.
43. Carol I, Prat P. A multicrack model based on the theory of multisurface plasticity and two fractures energies. *Proceedings of the IV Conference on Computational Plasticity*, Barcelona, 1999; 1583–1594.
44. Simo J, Hughes T. *Computational Plasticity*. Springer: New York, 1998.
45. UPC Geomechanical Group. *CODE_BRIGHT User's Manual*, 2004.
46. FEBEX Project. Full-scale engineered barriers experiment for a deep geological repository for high level radioactive waste in crystalline host rock. *Final Project Report*, *EUR 19612 EN*, European Commission, Brussels, 2000.
47. Sánchez M, Gens A. Second report on THM modelling results. FEBEX II. UPC Geomechanical Group. *ENRESA Report*: *70-UPC-L-5-011*, 2002.

